Applied Catalysis B: Environmental 255 (2019) 117749

Contents lists available at ScienceDirect

Applied Catalysis B: Environmental

journal homepage: www.elsevier.com/locate/apcatb

Promotional effect of Ce doping in $Cu_4Al_1O_x$ – LDO catalyst for low-T practical NH_3-SCR: Steady-state and transient kinetics studies

Qinghua Yan[a], Yanshan Gao[a], Yuran Li[b], Michalis A. Vasiliades[c], Sining Chen[a], Cheng Zhang[a], Rongrong Gui[a], Qiang Wang[a,*], Tingyu Zhu[b], Angelos M. Efstathiou[c,*]

[a] College of Environmental Science and Engineering, Beijing Forestry University, 35 Qinghua East Road, Haidian District, Beijing 100083, PR China
[b] Research Center for Process Pollution Control, National Engineering Laboratory for Hydrometallurgical Cleaner Production Technology, Institute of Process Engineering, Chinese Academy of Sciences, Beijing 100190, China
[c] Chemistry Department, Heterogeneous Catalysis Lab, University of Cyprus, 1 University Ave., University Campus, 2109 Nicosia, Cyprus

ARTICLE INFO

Keywords:
Selective catalytic reduction
Layered double hydroxides
SO_2 poisoning of NH_3-SCR
HCl poisoning of NH_3-SCR
Transient kinetics of NH_3-SCR

ABSTRACT

There are very few catalysts reported so far to withstand poisoning by the co-presence of SO_2, HCl and H_2O in the flue gas stream for the NH_3-SCR. The purpose of this work was to report for the first time, to the best of our knowledge, the development of a new catalyst, $Ce_2/Cu_4Al_1O_x$-layered double oxide (LDO) with high low-temperature de-NO_x activity and high poisoning resistance in the presence of H_2O, HCl and SO_2 in the feed gas stream. In particular, $Ce_2/Cu_4Al_1O_x$-LDO catalyst in the presence of 5% H_2O, 100 ppm HCl and 100 ppm SO_2 in the NH_3-SCR feed gas stream presented after 9 h of continuous reaction at 200 °C a relatively stable NO_x conversion (ca. 57.2%), where all other three control catalysts tested, namely: Cu/Al_2O_3, Cu-Ce/Al_2O_3 and $Cu_4Al_1O_x$ showed severe deactivation, where NO_x conversion values of ~0, 0 and 5.7%, respectively, were measured. It should be noted that the $Ce_2/Cu_4Al_1O_x$ catalyst achieved NO_x conversion of 95.3% at 200 °C in the absence of HCl and SO_2 in the feed gas stream. A suit of experimental techniques such as BET, XPS, ICS, *in situ* DRIFTS, pyridine- and NH_3-FTIR, NH_3-TPD, H_2-TPR and transient NH_3 chemisorption and NH_3-SCR kinetics were employed to reveal possible reasons for the high activity and poisoning resistance exhibited by the $Ce_2/Cu_4Al_1O_x$ catalytic system. XRD and XPS analyses showed that $Ce_2/Cu_4Al_1O_x$ had highly dispersed Cu^{2+} and Ce^{3+} species, which likely promote the rate of NH_3-SCR. Py-FTIR, NH_3-TPD and H_2-TPR results indicated that $Ce_2/Cu_4Al_1O_x$ has a larger concentration of surface acid sites and stronger redox properties. According to H_2-TPR, ICS and in-situ DRIFTS analyses, the redox properties of $Ce_2/Cu_4Al_1O_x$ were significantly less affected by the presence of HCl and SO_2 gases, and lower amounts of metal sulfate and metal chloride species were formed, thus proving its exhibited poisoning resistance. Transient kinetics experiments revealed that the larger site reactivity (k, s^{-1}) and NO oxidation rate to NO_2 and not the surface coverage of adsorbed NH_x-s active intermediates dictates the higher rate of NH_3-SCR over $Ce_2/Cu_4Al_1O_x$ compared to Cu/Al_2O_3 and Cu-Ce/Al_2O_3 non LDO- materials.

1. Introduction

The aftertreatment of NO_x-containing industrial flue gas streams by the ammonia selective catalytic reduction (NH_3-SCR) technology, usually involves large amounts of SO_x, chlorinated compounds and heavy metals in the flue gas streams [1–4]. Hydrogen chloride (HCl) and sulfur dioxide (SO_2) gases are usually observed in municipal and industrial solid waste incineration flue gas streams, which usually have an irreversible deactivation effect on the SCR catalysts. These two gases mainly arise from the combustion of sulfurous and halogenated organic wastes. The use of spraying alkaline absorbents and activated carbons are considered as the main measures to reduce the effect of SO_2 and HCl in traditional waste incinerators. However, the removal efficiency of these pollutants based on these measures is not the expected one, and both HCl and SO_2 may enter the SCR unit. Therefore, it becomes clear that practical working conditions require SCR catalysts to possess not only excellent low-T activity but also good resistance to SO_2 and HCl poisoning.

In the past several decades, various catalysts have been studied for the selective conversion of NO_x into N_2 in a flue gas containing also HCl and/or SO_2, including supported noble metals [5,6], zeolites [7] and metal oxide catalysts [8,9]. Supported noble metal catalysts have better activity but their use is rather limited due to their high cost, low N_2-selectivity and extreme vulnerability to SO_2. Zeolite catalysts have poor

* Corresponding authors.
E-mail addresses: qiangwang@bjfu.edu.cn (Q. Wang), efstath@ucy.ac.cy (A.M. Efstathiou).

https://doi.org/10.1016/j.apcatb.2019.117749
Received 25 February 2019; Received in revised form 10 May 2019; Accepted 14 May 2019
Available online 15 May 2019

hydrothermal stability, and their framework is easy to collapse in the presence of acidic gases such as HCl and SO_2. Metal oxide catalysts have become a hotspot of research due to their wide-temperature window of operation and relatively better stability for practical applications.

In order to improve the resistance of NH_3-SCR catalysts to HCl and/or SO_2 poisons, several strategies have been reported. One strategy is to use additional metal components in the case of metal oxide catalysts, such as Co, Ni, Cu, Cr, Fe, V or Ce [8–14]. The individual influence of either SO_2 or HCl has been studied in recent years [5,11]. Du et al. [13] found that after adding Cu to Ce-Ti-O mixed metal oxide can result in an improved SO_2 resistance. Chen et al. [14] revealed that the SO_2 resistance and catalytic activity of MnO_x could be increased by the addition of Cr metal in MnO_x. Yao et al. [15] prepared CeO_2@Ce-O-P and found that the formation of a Ce-O-P shell increased the amount of acid sites, and thus avoided the adsorption of SO_2 on the catalyst surface. Lian et al. [16] observed the improvement of SO_2-resistance of VO_x/CeO_2 catalyst by Nb addition to the catalyst composition. Salem et al. [17] demonstrated that adding ZrO_2 and SnO_2 can enhance the de-NO_x activity and SO_2 resistance of a Pt/Al_2O_3 catalyst. Choung et al. [18,19] and Park et al. [20] reported that the introduction of Ce into Cu ion-exchanged mordenite zeolite catalysts improves the HCl-resistance of catalyst. Chang et al. [21] found that CeO_2-MoO_3 catalysts possess certain resistance to HCl and H_2O at 200 °C.

Most of the above mentioned studies concern only one pollutant, either SO_2 [22,23] or HCl [18,19]. However, in many cases, both HCl and SO_2 co-exist in several flue gas streams. It should be noted that the poisoning effect of the co-existence of HCl and SO_2 appears more complicated for practical applications of SCR catalysts. More precisely, Chang et al. [6] found that the catalytic performance of Rh/Al_2O_3 and Rh-Na/Al_2O_3 towards NO_x conversion was largely reduced at high concentrations of HCl and SO_2, where the poisoning effect of HCl was even higher than that of SO_2.

To the best of our knowledge, reports on improving the deactivation of NH_3-SCR catalysts due to the existence of both HCl and SO_2 poisons in the NO_x-containing flue gas streams are still very rare, particularly in the presence of water vapor. Therefore, it is highly desirable to design and develop robust catalytic systems for low-temperature NH_3-SCR in the presence of HCl, SO_2 and water vapor, and to also understand possible mechanisms of their catalyst deactivation effects.

Layered double hydroxides (LDHs) and layered double oxides (LDOs) have been widely studied in many different fields due to their unique structure and properties, to mention electronic properties as supercapacitors [24], CO_2 capture efficiency [25], catalytic oxidation of VOCs [26], and two-dimensional membrane structure for gas and liquid separations [27]. Recently, we reported that $Cu_1Mn_{0.5}Ti_{0.5}O_x$ – layered double oxide (LDO) catalyst, formed after calcination of layered double hydroxides (LDHs), exhibits excellent NH_3-SCR performance in the presence of SO_2 [28]. Due to the unique layered structure of LDHs materials, the active components are highly dispersed within the layered double oxides [29,30]. In addition, Ce-based catalysts are considered as suitable alternatives to commercial V_2O_5-WO_3/TiO_2 SCR catalysts due to their excellent redox and labile oxygen mobility properties [31,32]. Pure CeO_2, however, exhibits poor thermal stability that leads to sintering.

In the present work, CeO_{2-x} nanoparticles were deposited on $Cu_4Al_1O_x$-LDO support and the resulting solid was investigated towards low-temperature NH_3-SCR. Of particular interest was the individual/co-existence effects of HCl and/or SO_2 on the NH_3-SCR activity and N_2-selectivity of $Ce_y/Cu_4Al_1O_x$-LDO solids. A strict comparison of the activity of the latter catalysts was attempted against Cu/Al_2O_3, Cu-Ce/Al_2O_3 and $Cu_4Al_1O_x$-LDO solids, where the former two catalysts were prepared by the standard wet impregnation method. The influence of Ce content, reaction temperature and the co-presence of HCl and SO_2 along with H_2O on the de-NO_x performance of catalysts were investigated. Transient kinetics studies of NH_3 chemisorption, NH_3-SCR and adsorbed NO_x stability in the presence of 5 vol% O_2 at 150 and 200 °C using mass spectrometry, conducted for the first time, to the best of our knowledge, over LDO-type of materials, largely provided a better understanding of the role of Ce in the $Ce_y/Cu_4Al_1O_x$ and Cu-Ce/Al_2O_3 catalysts.

2. Experimental

2.1. Catalysts preparation

The Cu_4Al_1-CO_3 LDHs (with Cu/Al molar ratio of 4:1) were synthesized by a co-precipitation method. For Ce_y/Cu_4Al_1-CO_3 LDHs (Cu/Al molar ratio of 4:1; Cu/Ce molar ratio of 4:0.5, 4:1, 4:2, 4:3; y = 0.5, 1, 2, 3), Ce was introduced during the Cu_4Al_1-CO_3 LDH co-precipitation synthesis step. First, the aqueous solution with corresponding amounts of $Al(NO_3)_3{\cdot}9H_2O$, $Cu(NO_3)_2{\cdot}6H_2O$ and $Ce(NO_3)_3{\cdot}6H_2O$ was uniformly added dropwise to a vigorous stirring Na_2CO_3 aqueous solution. The pH value of 10 of the resulting liquid mixture was maintained by adding NaOH (4 M) solution. The slurry obtained was further aged for 12 h, and filtered by deionized water to pH = 7. The slurry containing Ce_y/Cu_4Al_1-CO_3 LDHs and Cu_4Al_1-CO_3 LDH was further washed with acetone and then dried at 60 °C. The dried samples were described as Ce_y/Cu_4Al_1-CO_3 LDHs (y = 0.5, 1, 2, 3) and Cu_4Al_1-CO_3 LDH. Finally, the latter materials were subjected to calcination at 400 °C for 5 h to obtain the corresponding $Cu_4Al_1O_x$-LDO and $Ce_y/Cu_4Al_1O_x$-LDO catalysts. 10 wt% CuO/Al_2O_3 (denoted as Cu/Al_2O_3) and 5 wt% CuO-5 wt% CeO_2/Al_2O_3 (denoted as Cu-Ce/Al_2O_3) were synthesized following the standard wet impregnation method and these materials were used as control NH_3-SCR catalysts.

2.2. Catalysts characterization

The catalyst samples were characterized for their solid crystal phases using powder X-ray diffraction (XRD-7000, Shimadzu, Cu Kα radiation). The specific surface area (SSA, $m^2\,g^{-1}$) of catalysts was determined by N_2 adsorption/desorption analysis at 77 K (SSA-7000, Builder). Surface chemical composition and oxidation states of elements were determined by X-ray photoelectron spectroscopy (XPS) analyses (Thermo Scientific Escalab 250Xi instrument) using monochromatic Al Kα radiation (hν = 1486.6 eV) with an accelerating power of 15 kW. The surface acidity of the solids was determined by NH_3-temperature programmed desorption (NH_3-TPD) and their redox properties by H_2-temperature programmed reduction (H_2-TPR) both conducted on a multifunction chemisorption analyzer (PCA-1200, Builder). First, the solids were pretreated in Ar (30 mL/min) at 400 °C for 30 min before performing the NH_3-TPD and H_2-TPR experiments. For H_2-TPR, the solids were heated from 50 to 800 °C (10 °C/min) in 5% H_2/Ar gas mixture (30 mL/min). For NH_3-TPD, the solids were saturated with pure NH_3 (30 mL/min) at 80 °C for 30 min, and then heated in Ar gas flow at the rate of 10 °C/min over the temperature range of 80–800 °C.

After the pre-chlorination treatment, the amount of deposited Cl ions (mg Cl g^{-1}) on the Cu/Al_2O_3, Cu-Ce/Al_2O_3, $Cu_4Al_1O_x$ and $Ce_2/Cu_4Al_1O_x$ catalysts was estimated using ion chromatography (ICS-1100, Thermo Dionex). Table 1 shows the Cl content in catalysts after the pre-chlorination treatment.

FTIR spectra of chemisorbed pyridine (Py-FTIR) were recorded and analyzed using a Thermo Nicolet 380 FTIR spectrometer. Isothermal adsorption of pyridine was conducted at 200 °C and IR spectra were collected every 1 min, and the total amount of Lewis and Brönsted acid sites was quantitatively calculated by integrating the respective infrared absorption band intensity related to the Lewis and Brönsted acid sites based on the quantitative analysis reported (determination of integrated molar extinction coefficient of adsorbed pyridine) [33].

In situ DRIFTS studies were conducted using a commercial environmental chamber (Harrick) served as reaction cell (ZnSe window) and an FTS 3000 MX FTIR spectrophotometer (Bruker Vertex 70). The Kubelka-Munk (KM) function was selected to report the IR spectral data

Table 1
Textural properties (SSA, pore size and pore volume), XPS analyses and the total content of Cl (determined by ion chromatography) of Cu/Al_2O_3, $Cu\text{-}Ce/Al_2O_3$, $Cu_4Al_1O_x$ and $Ce_y/Cu_4Al_1O_x$ catalysts.

Catalysts	BET SSA (m^2/g)	BJH pore size (Å)	BJH pore volume (cm^3/g)	$Cu^{2+}/(Cu^{2+}+Cu^{+})$	$Ce^{3+}/(Ce^{3+}+Ce^{4+})$	$O_\beta/(O_\beta+O_\alpha)$	Total Cl content (mg/g)
Cu/Al_2O_3	76.7	54.9	0.37	0.55	–	0.57	1.81
$Cu\text{-}Ce/Al_2O_3$	66.4	48.5	0.54	0.67	0.11	0.63	0.99
$Cu_4Al_1O_x$	125.1	95.1	0.6	0.8	–	0.65	0.76
$Ce_{0.5}/Cu_4Al_1O_x$	130.8	131.4	0.86	–	–	–	–
$Ce_1/Cu_4Al_1O_x$	137.2	114.4	0.79	–	–	–	–
$Ce_2/Cu_4Al_1O_x$	173.0	109.6	0.95	0.87	0.45	0.7	0.56
$Ce_3/Cu_4Al_1O_x$	136.7	110.5	0.69	–	–	–	–

obtained, whereas the background spectrum of the solid was recorded in N_2 gas atmosphere at the temperature of interest, and which was subtracted from the spectrum of the solid recorded under the gas atmosphere of interest. The number of scans was set to 32, and the resolution used for the analysis was set to 4 cm^{-1}.

2.3. Catalytic activity measurements

The catalytic activities of solid samples were evaluated in a fixed-bed stainless steel micro-reactor loaded with 150 mg of solid. The total volume flow rate used was 200 N mL/min, resulting in a GHSV of 60,000 h^{-1}. The feed gas composition consisted of 500 ppm NH_3, 500 ppm NO_x (~ 480 ppm NO and 20 ppm NO_2), 5% O_2, 5% H_2O (if needed), 100 ppm SO_2 (if needed) and 100 ppm or 200 ppm HCl (if needed) with Ar gas as balance. The MultiGas 2000 analyzer (MKS, USA) was used to monitoring the concentration of NO_x (NO/NO_2), N_2O and NH_3. The following Eqs. (1) and (2) were used to estimate the NO_x conversion and N_2 selectivity:

$$NO_x \quad \text{conversion} = \left(1 - \frac{NO_x(out)}{NO_x(in)}\right) \times 100\% \tag{1}$$

$$\text{N}_2 \quad \text{selectivity} = \left(1 - \frac{2\text{N}_2\text{O}(out)}{NO_x(in) + \text{NH}_3(in) - NO_x(out) - \text{NH}_3(out)}\right) \times 100\% \tag{2}$$

Catalytic measurements in the temperature range of 100–250 °C (50 °C per step) were obtained after 1 h in $NH_3/NO/O_2/N_2$ feed gas stream at each reaction temperature.

2.4. Various transient kinetics experiments for the NH_3-SCR

The transient adsorption kinetics behavior of NH_3 and NO and the transient NH_3-SCR kinetics of the most active and least active Ce_2/Cu_4AlO_x and Cu/Al_2O_3 catalysts, respectively, identified under steady-state NH_3-SCR conditions, was investigated according to the following step-gas switches performed at T = 150 and 200 °C:

(i) Ar/He → 1000 ppm NH_3/1%Kr/Ar/He (T, t)
(ii) 1000 ppm NH_3/Ar/He (20 min, T) → 1000 ppm NO/5% O_2/1% Kr/Ar/He (T, t)
(iii) He → 1000 ppm NO/5% O_2/1% Kr/Ar/He (T, t)
(iv) He → 1000 ppm NO/1% Kr/Ar/He (T, t)
(v) 1000 ppm NO/1% Kr/Ar/He (T, 20 min) → 5% O_2/He (T, t)

These transient experiments were conducted in a specially designed transient gas-flow system and using a CSTR micro-reactor previously described [34]. The effluent gas stream from the micro-reactor was continuously monitored by an *on-line* mass spectrometer (Balzers, Omnistar, 1–300 amu). The mass numbers (*m/z*): 16 (or 15), 28, 30, 44, 46 and 84 were used to monitor NH_3, N_2, NO, N_2O, NO_2 and Kr gases. The preset gas composition of NH_3 and NO in the feed gas streams, as well as the composition of the product gases at the exit stream from the micro-reactor were estimated by using certified gas mixtures, ca. 1000 ppm NH_3/He, 1.0 vol%N_2/He, 984 ppm NO/He, 144 ppm N_2O/He and 180 ppm NO_2/1%O_2/He for the calibration of the respective MS signal recorded.

At the switch Ar/He → 1000 ppm NH_3/1%Kr/Ar/He (T, t), NH_3 is adsorbed on surface acidic sites of the solid but it could also react with surface oxygen of the mixed metal oxide catalyst. The transient rate of ammonia consumption (R_{NH3}) was calculated using the appropriate material balance for the CSTR micro-reactor used, described by the following Eq. (3), while the amount of ammonia consumption (mol g^{-1}) was estimated after integration of the rate vs time response curve obtained. The accumulation term in the material balance was neglected since this was found to be very small compared to the other two terms shown in the right-hand side of Eq. (3).

$$R_{\text{NH}_3}\ (\text{mol}\quad \text{g}^{-1}\quad \text{s}^{-1}) = \frac{F_T}{W} y^f_{\text{NH}_3} (Z_{\text{Kr}}(t) - Z_{\text{NH}_3}(t)) \tag{3}$$

In Eq. (3), Z_{Kr} and Z_{NH3} are the dimensionless concentrations of Kr tracer gas and NH_3, respectively, where Z_i (t) = y_i (t)/y_i^f. Here, y_i (t) is the mole fraction of Kr or NH_3 at a given time during the transient chemisorption experiment, and y_i^f is the mole fraction corresponding to the feed composition at the gas step switch. Thus, Z_i = 1.0 when the Kr signal or the NH_3 signal in the mass spectrometer takes the corresponding value of 1 mol% or 1000 ppm in the feed. Similar analysis for the determination of the transient rate of NO consumption (R_{NO}) during the step-gas switches (iii) and (iv) described above was made, and corresponding relationship to that given by Eq. (3) for the R_{NO} can be derived.

During the gas-switch (ii), pre-adsorbed NH_3-s species corresponding to an almost full surface coverage at the corresponding T (150 or 200 °C) of adsorption, react under the NO/O_2/He/Kr/Ar gas mixture (NH_3-SCR) leading to N_2 and N_2O (no NO_2 was detected). At the same time, NO_x adsorbed species are formed, the amount (μmol g^{-1}) of which can be estimated via a material balance described by Eq. (4):

$$NO_x - s(\mu\text{mol}\quad \text{g}^{-1}) = [\text{NO} - consumed] - ([\text{N}_2\quad formed] + [\text{N}_2\text{O}\quad formed]) \tag{4}$$

It should be noted that 1 mol NO reacted corresponds to 1 mol N_2 or N_2O formed based on the standard NH_3-SCR described by Eqs. (5) and (6):

$$4NH_3 + 4NO + O_2 \rightarrow 4N_2 + 6H_2O \tag{5}$$

$$4NH_3 + 4NO + 3O_2 \rightarrow 4N_2\,O + 6H_2O \tag{6}$$

The rate of NO consumption was estimated according to Eq. (7), while that of NH_3 desorption, N_2, N_2O or NO_2 gas production according to Eq. (8).

$$R_{\text{NO}}\ (\text{mol}\quad \text{g}^{-1}\quad \text{s}^{-1}) = \frac{F_T}{W} y^f_{\text{NO}} (Z_{\text{Kr}}(t) - Z_{\text{NO}}(t)) \tag{7}$$

$$R_i\ (\text{mol}\quad \text{g}^{-1}\,\text{s}^{-1}) = \frac{F_T}{W} y_i(t) \tag{8}$$

Integration of the R_{NO}, R_{N2} and R_{N2O} transient curves with time provides the corresponding amount (μmol g^{-1}) of consumed or produced species.

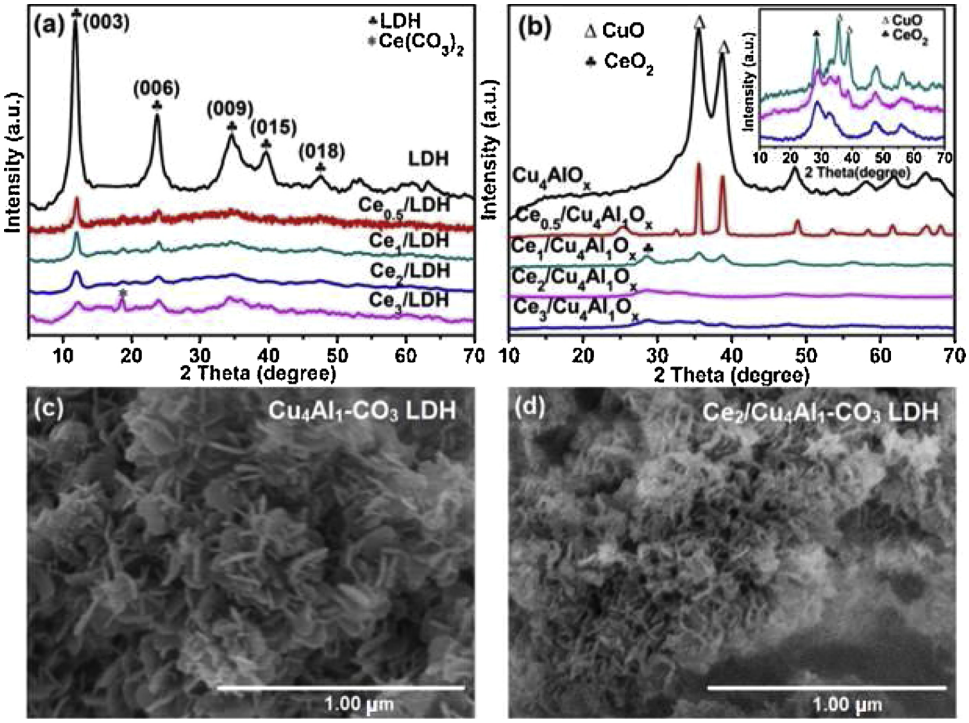

Fig. 1. XRD patterns of Ce_y/Cu_4Al_1-CO_3 LDHs (a) and $Ce_y/Cu_4Al_1O_x$ solids (b); SEM images of Cu_4Al_1-CO_3 LDH (c) and Ce_2/Cu_4Al_1-CO_3 LDH (d) solids.

3. Results and discussion

3.1. Structural and textural characterization of catalysts

The successful syntheses of Ce_y/Cu_4Al_1-CO_3 and Cu_4Al_1-CO_3 LDH precursor materials were checked by powder XRD analyses (Fig. 1a). It can be seen that all the Ce_y/Cu_4Al_1-CO_3 samples show similar typical layered structure to hydrotalcite [35,36]. The characteristic diffraction peaks of Cu_4Al_1-CO_3 LDH are observed at 2θ = 11.82°, 23.72°, 34.62°, 39.6° and 47.66°, corresponding to reflections from the (003), (006), (012), (015) and (118) crystal faces, respectively. For the series of Ce_y/Cu_4Al_1-CO_3 LDHs, a diffraction peak at 17° is observed, suggesting that Ce is mainly present as $Ce(CO_3)_2$ (JCPDS No. 22-0542). Fig. 1b indicates that after calcination at 400 °C, both Cu_4Al_1-CO_3 and Ce_y/Cu_4Al_1-CO_3 LDHs solids were transformed into a mixture of spinels and metal oxides. For $Cu_4Al_1O_x$-LDO, there are two main diffraction peaks (~ 35.5° and 38.7°) assigned to CuO (JCPDS No. 48-1548). With the introduction of Ce ($Ce_2/Cu_4Al_1O_x$), diffraction peaks assigned to CeO_2 cubic structure (JCPDS No. 34-0349) appear (see inset Fig. 1b). In the XRD pattern of Cu-Ce/Al_2O_3 (Fig. S1a), no diffraction peaks belonging to CuO/Cu_2O and $CeO_{2-\delta}$ phases were observed, which indicates that the Cu and Ce species mainly existed in a highly dispersed amorphous state and/or in oxidic form with mean particle size smaller than 4 nm (not detected by powder XRD).

The morphology of Cu_4Al_1-CO_3 and Ce_2/Cu_4Al_1-CO_3 LDHs was also explored using SEM analyses (Fig. 1c, d). Cu_4Al_1-CO_3 LDH displays typical "flower-like" morphology [37]. After introducing Ce, less crystallized nanoplatelets are observed in the Ce_2/Cu_4Al_1-CO_3 LDH (Fig. 1d). Since Ce^{4+} has a cationic size larger than the spacing of LDH brucite layers, it cannot enter the space but instead it is expected to be found on the surface of LDHs. The morphology and nano-structure of Ce_2/Cu_4Al_1-CO_3 LDH and $Ce_2/Cu_4Al_1O_x$-LDO solids were further explored by HR-TEM analyses. For Ce_2/Cu_4Al_1-CO_3 LDH, a "flower-like" layered morphology is observed (Fig. 2a). After calcination at 400 °C, there was almost no change in the morphology of $Ce_2/Cu_4Al_1O_x$ (Fig. 2b), which is similar to that of Ce_2/Cu_4Al_1-CO_3 LDH. The SEM images for $Cu_4Al_1O_x$-LDO and Cu-Ce/Al_2O_3 catalysts are shown in Fig. S1b-c, where $Cu_4Al_1O_x$-LDO showed nanosheet morphology (Fig. S1b), while Cu-Ce/Al_2O_3 showed irregular aggregated particles (Fig. S1c). Furthermore, highly crystalline lattice with fringe spacings of 0.31 and 0.25 nm appear, which belong to the (111) crystal face of CeO_2 and (-111) face of CuO, respectively (Fig. 2c) [15,28,38]. These results agree well with the powder XRD patterns shown in Fig. 1b, where the characteristic diffraction peaks of CeO_2 and CuO single phases are clearly identified. The presence of Ce and Cu species was also confirmed by TEM-EDS analysis (Fig. 2d). The existence of CuO_x and CeO_x species in $Ce_2/Cu_4Al_1O_x$ were confirmed by mapping analysis (Fig. 2e, f), showing that CuO_x and CeO_x are in highly dispersed states.

The textural properties of $Ce_y/Cu_4Al_1O_x$-LDO, Cu-Ce/Al_2O_3 and Cu/Al_2O_3 solids were investigated by BET analyses (Table 1). Apparently, $Ce_2/Cu_4Al_1O_x$ has the largest SSA (173 m^2/g) and pore volume (0.95 cm^3/g), with Cu/Al_2O_3 to have the smallest SSA (76.7 m^2/g) and pore volume (0.37 cm^3/g). Since the activity of the $Ce_y/Cu_4Al_1O_x$-LDO solids is associated with the surface concentration of Ce and Cu species, it is reasonable to suggest that the SSA can partly explain the high activity on a gram-basis observed in these materials (Section 3.2).

3.2. NH_3-SCR performance of $Ce_y/Cu_4Al_1O_x$ solids

In order to determine an optimal Cu/Ce ratio for the NH_3-SCR conducted over the $Ce_y/Cu_4Al_1O_x$ solids, the NO_x conversion and N_2-selectivity behavior in the temperature range of 100–250 °C was studied. Fig. 3a clearly shows that the $Ce_2/Cu_4Al_1O_x$ catalyst exhibits the best NH_3-SCR activity, especially at low temperatures (T < 200 °C). The maximum NO_x conversion decreases in the order: $Ce_2/Cu_4Al_1O_x$ (95.3%) > $Ce_1/Cu_4Al_1O_x$ (93.3%) > $Ce_{0.5}/Cu_4Al_1O_x$ (92.5%) > $Cu_4Al_1O_x$ (91.1%) > $Ce_3/Cu_4Al_1O_x$ (88.6%) > Cu-Ce/Al_2O_3 (87.9%) > Cu/Al_2O_3 (82.6%). Based on these results, an optimal *y* value of 2 was determined, where further increase of the *y* value (from 2 to 3) leads to an obvious activity decline. This might be attributed to the maximum loading of support [39,40]. When the loading of the active component exceeds the maximum loading of support, the sintering problem easily occurs, thereby affecting the performance of the catalyst. By contrast, Cu/Al_2O_3 exhibits a small low-T (T = 100 °C) activity, with the highest NO_x conversion (82.6%) to be

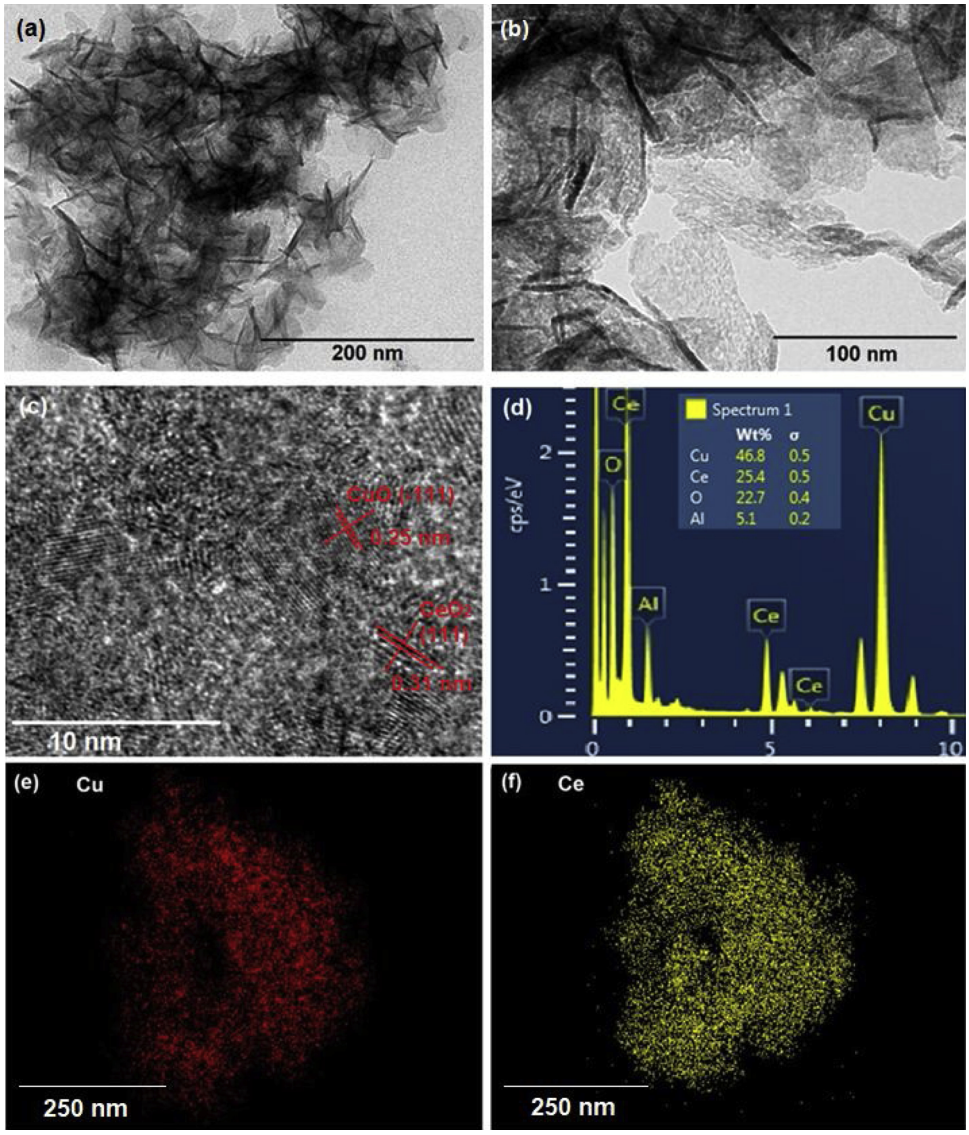

Fig. 2. HR-TEM images of Ce_2/Cu_4Al_1-CO_3 LDH (a) and $Ce_2/Cu_4Al_1O_x$ (b, c) solids. (d) TEM-EDS analysis of $Ce_2/Cu_4Al_1O_x$ solids. EDS elemental mapping of Cu in $Ce_2/Cu_4Al_1O_x$ (e) and Ce in $Ce_2/Cu_4Al_1O_x$ (f).

obtained at 250 °C.

Fig. 3b shows the change in NO_x conversion when 5% H_2O is introduced in the feed gas stream over the series of $Ce_y/Cu_4Al_1O_x$ catalysts. In the H_2O tolerance test performed at 200 °C, the NO_x conversion for the $Ce_2/Cu_4Al_1O_x$ catalyst is the highest (82.8%) among $Cu_4Al_1O_x$ (75%), Cu-Ce/Al_2O_3 (68.7%) and Cu/Al_2O_3 (66%), indicating that $Ce_2/Cu_4Al_1O_x$-LDO catalyst exhibits the best activity drop resistance to H_2O. It is interesting to note that a drop in activity by only 12.5%-units is observed at 200 °C over the $Ce_2/Cu_4Al_1O_x$ catalyst.

Since the side reaction of NH_3 oxidation might had been occurred during the NH_3-SCR, the N_2-selectivity behavior of the catalysts in the presence of 5% H_2O is reported in Fig. 3c. It can be seen that Cu/Al_2O_3 displays the lowest N_2-selectivity value as opposed to $Ce_2/Cu_4Al_1O_x$, which shows the highest one in the 100–250 °C range. Fig. S2 shows the N_2-selectivity of the same series of catalysts in the absence of H_2O at 100–250 °C, under which $Ce_2/Cu_4Al_1O_x$ still exhibits higher N_2-selectivity. Therefore, it is demonstrated that the N_2-selectivity in the presence/absence of H_2O for the $Cu_4Al_1O_x$ catalyst was enhanced after the introduction of Ce. In addition, $Ce_2/Cu_4Al_1O_x$ shows good performance in the presence of 5% H_2O in the feed at higher GHSVs. By changing the GHSV from 60,000 to 105,000 h^{-1}, the NO_x conversion of $Ce_2/Cu_4Al_1O_x$ was found to only slightly decrease (Fig. 3d). In particular, at 200 °C (maximum conversion is observed), the NO_x conversion of $Ce_2/Cu_4Al_1O_x$ in the presence of 5% H_2O decreases only slightly, ca. from 82.8 to 73.5%, as opposed to that of Cu/Al_2O_3, which decreases significantly, ca. from 66 to 46.4%.

The above results demonstrate that the introduction of Ce in the $Cu_4Al_1O_x$-LDO increases both the reaction rate and N_2-selectivity of the NH_3-SCR, and at the same time widens the operating T-window of the Cu-based catalyst (Fig. 1b, d). In the transient kinetics studies (Section 3.6) we examined the transient NH_3 chemisorption and transient NH_3-SCR of $Ce_2/Cu_4Al_1O_x$ and Cu-Ce/Al_2O_3 catalysts at 150 and 200 °C. The results show that the $Ce_2/Cu_4Al_1O_x$ has a higher NH_3 chemisorption rate, a faster NO_x consumption rate, and a higher N_2 production rate, which are also consistent with the steady-state results of the catalytic activity.

3.3. HCl and/or SO_2 resistance to activity drop and regeneration of catalysts

The poisoning effects of HCl and SO_2 are mainly attributed to their interaction with the active metal or support surface towards the

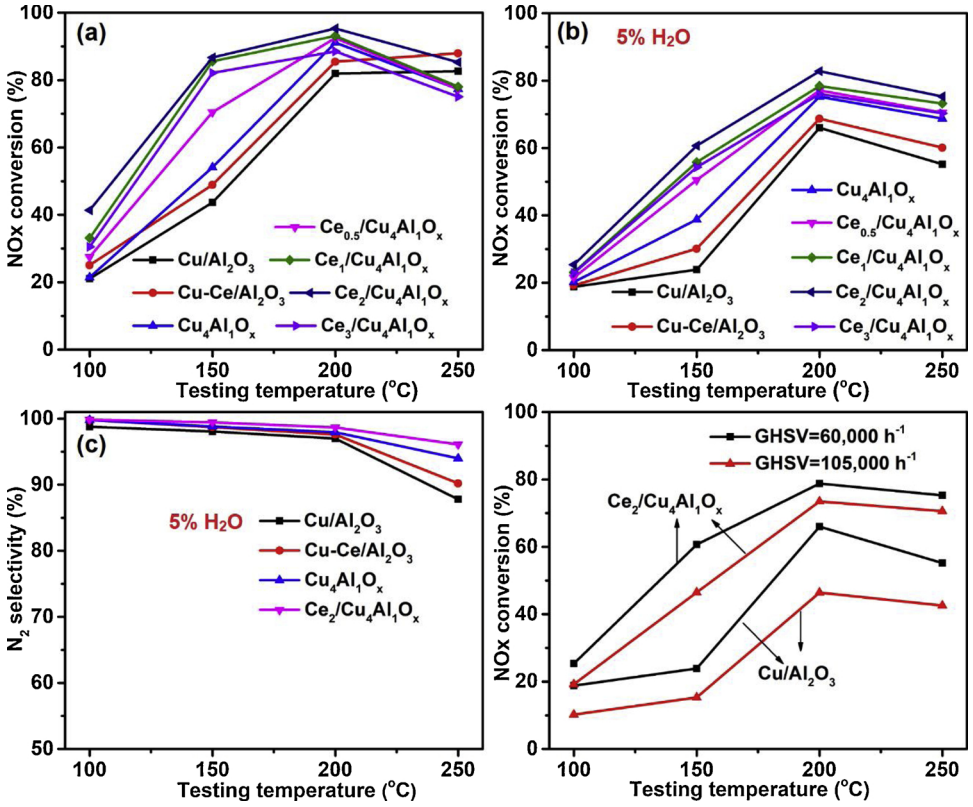

Fig. 3. NO_x conversions over catalysts as a function of temperature without the presence of H_2O in the feed (a), and in the presence of 5% H_2O in the feed (b). (c) N_2-selectivity of catalysts in NH_3-SCR at different temperatures and in the presence of 5% H_2O in the feed. (d) NO_x conversion over $Ce_2/Cu_4Al_1O_x$ and Cu/Al_2O_3 catalysts under different GHSV (60,000 h^{-1} and 105,000 h^{-1}) in the presence of 5% H_2O in the feed. Reaction conditions: $[NO_x] = [NH_3]$ = 500 ppm, $[O_2]$ = 5%, $[H_2O]$ = 5%, balance Ar, total flow rate = 200 mL/min, GHSV = 60,000 h^{-1}, W_{cat} = 0.15 g.

formation of metal sulfates and metal chlorides. Fig. 4a shows the effect of HCl and H_2O on the NO_x conversion of $Ce_y/Cu_4Al_1O_x$-LDO, Cu/Al_2O_3 and $Cu\text{-}Ce/Al_2O_3$ catalysts as a function of reaction temperature. With the presence of 100 ppm HCl and 5% H_2O in the feed gas stream, the NO_x conversion of $Ce_2/Cu_4Al_1O_x$ at 200 °C (75.2%) appears much higher than that of Cu/Al_2O_3 (30.5%), $Cu\text{-}Ce/Al_2O_3$ (35.4%) and $Cu_4Al_1O_x$ (55.6%). By increasing the HCl concentration to 200 ppm, the NO_x conversion of all catalysts decreases (Fig. 4b). In particular, the NO_x conversion at 200 °C of $Ce_2/Cu_4Al_1O_x$ (70.2%) is still significantly higher than that of Cu/Al_2O_3 (18.8%), $Cu\text{-}Ce/Al_2O_3$ (25.4%) and $Cu_4Al_1O_x$ (30.2%). At lower (150 °C) and higher (250 °C) temperature, the $Ce_2/Cu_4Al_1O_x$-LDO catalyst also appears more resistant to HCl (100 ppm) than the rest of the catalysts (Fig. 4a). Therefore, it could be concluded that introduction of Ce in the $Cu_4Al_1O_x$-LDO solid indeed

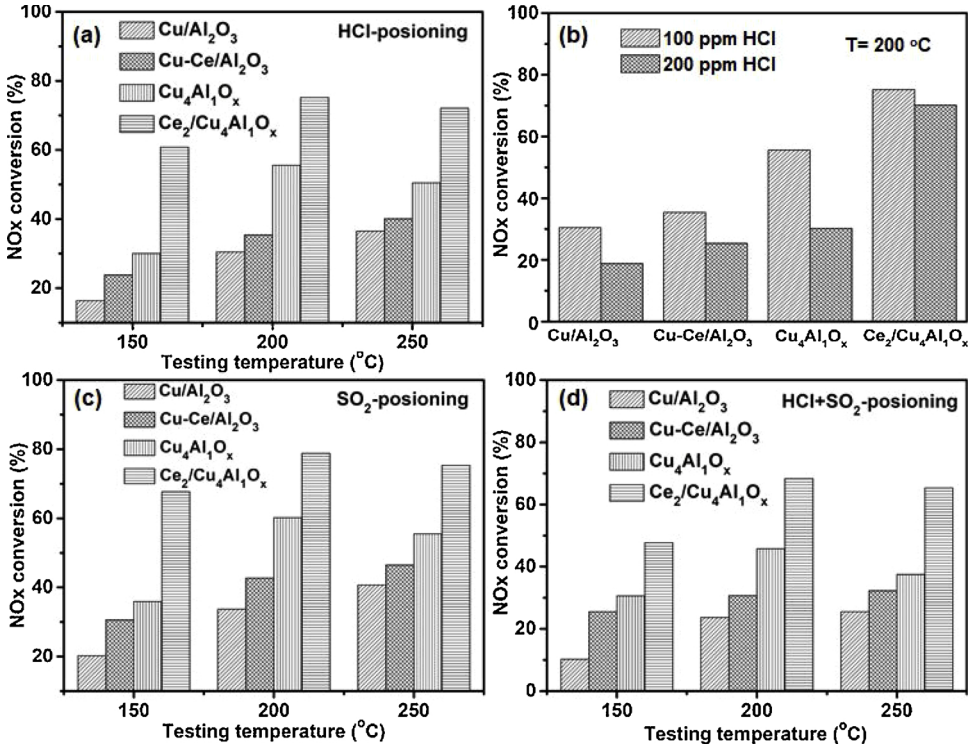

Fig. 4. The effect of 100 ppm HCl (a), different concentration of HCl (b), 100 ppm SO_2 (c) and 100 ppm HCl and 100 ppm SO_2 co-existence (d) on the NO_x conversion over the various catalysts. Reaction conditions: $[NO_x] = [NH_3]$ = 500 ppm, $[O_2]$ = 5%, $[H_2O]$ = 5%, [HCl] = $[SO_2]$ = 100 ppm, balance Ar, total flow rate = 200 mL/min, GHSV = 60,000 h^{-1}, W_{cat} = 0.15 g.

mitigate the effect of HCl poisoning in NH_3-SCR and in the presence of 5% H_2O in the feed gas stream.

The influence of 100 ppm SO_2 in the presence of 5% H_2O in the NH_3-SCR on the NO_x conversion over the $Ce_y/Cu_4Al_1O_x$-LDO, Cu/Al_2O_3 and $Cu\text{-}Ce/Al_2O_3$ catalysts after 1 h on reaction stream is presented in Fig. 4c. At 200 °C, the NO_x conversion of $Ce_2/Cu_4Al_1O_x$ appears as high as 78.8%, which is significantly higher than that of Cu/Al_2O_3 (33.7%), $Cu\text{-}Ce/Al_2O_3$ (42.7%) and $Cu_4Al_1O_x$ (60.2%). Similar results were obtained at 150 °C and 250 °C (Fig. 4c), which all demonstrate that the introduction of Ce in the $Cu_4Al_1O_x$-LDO structure can largely enhance the SO_2 resistance to activity drop for the $Ce_2/Cu_4Al_1O_x$ catalyst. The present results also indicate that HCl caused more severe deactivation than SO_2, which is consistent with literature reports [7,41].

In many flue gas compositions, both HCl and SO_2 are present but their overall influence, particularly in the presence of H_2O, has been rarely investigated. Fig. 4d compares the NO_x conversion obtained over $Ce_2/Cu_4Al_1O_x$, Cu/Al_2O_3, $Cu\text{-}Ce/Al_2O_3$, and $Cu_4Al_1O_x$ catalysts for a flue gas containing 5% H_2O, 100 ppm HCl and 100 ppm SO_2 at 150, 200 and 250 °C and after 1 h on reaction stream. The co-presence of HCl and SO_2 appears to show a synergistic deactivation effect on the NO_x conversion in NH_3-SCR for all four catalysts. In the case of Cu/Al_2O_3, $Cu\text{-}Ce/Al_2O_3$ and $Cu_4Al_1O_x$, the NO_x conversion at 200 °C drops significantly from 81.9, 85.4 and 91.1% to 23.7, 30.7 and 45.8%, respectively. However, under the same reaction conditions, $Ce_2/Cu_4Al_1O_x$-LDO still presents a large NO_x conversion (68.3%). The effects of 100 ppm SO_2 and 100 ppm HCl on $Ce_2/Cu_4Al_1O_x$ and $Cu\text{-}Ce/Al_2O_3$ catalysts performance in the absence of H_2O were also evaluated and results are shown in Fig. S3. The effect of SO_2 and HCl on the catalysts was relatively small compared to the conditions in which H_2O was present. It is illustrated that the introduction of Ce in the $Ce_2/Cu_4Al_1O_x$-LDO solid composition can significantly improve its activity drop resistance to HCl and SO_2 in the presence or the absence of H_2O in the feed stream.

The long-term de-NO_x performance stability and the regeneration ability of practical SCR catalysts are crucial. Fig. 5a presents the NO_x conversion behavior with time on stream (up to 9 h) of $Ce_2/Cu_4Al_1O_x$-LDO catalyst in the co-presence of HCl, SO_2 and H_2O along with that of the other three control catalysts: Cu/Al_2O_3, $Cu\text{-}Ce/Al_2O_3$ and $Cu_4Al_1O_x$-LDO. During the first 2 h, $Ce_2/Cu_4Al_1O_x$ shows a relatively obvious decline in NO_x conversion, ca. from 80 to 65%. After that, the NO_x conversion becomes very stable, with a slight decrease only, from 65 to 57.2% after 9 h on reaction stream. On the other hand, all other three control catalysts deactivate severely, where the NO_x conversion of Cu/Al_2O_3, $Cu\text{-}Ce/Al_2O_3$ and $Cu_4Al_1O_x$-LDO decreases to 0, 0, and 5.7%, respectively, after 9 h on reaction stream. These important results indicate that $Ce_2/Cu_4Al_1O_x$-LDO catalyst has superior activity drop resistance to the simultaneous presence of HCl, SO_2 and H_2O in the NH_3-SCR process.

Fig. 5b presents the ability of regeneration of the poisoned SCR catalysts of investigation. It is recalled that the fresh Cu/Al_2O_3, $Cu\text{-}Ce/Al_2O_3$, $Cu_4Al_1O_x$ and $Ce_2/Cu_4Al_1O_x$ catalysts present NO_x conversion values at 200 °C of 81.9, 85.4, 91.1 and 95.3%, respectively. Once 100 ppm SO_2, 100 ppm HCl and 5% H_2O were introduced into the feed gas stream for 4 h, the NO_x conversion declines to 6.4, 17.6, 23.9 and 60.3%, respectively. Subsequently, after the poisoned catalysts were thermally regenerated in air at 400 °C/5 h, the NO_x conversion of Cu/Al_2O_3, $Cu\text{-}Ce/Al_2O_3$, $Cu_4Al_1O_x$ and $Ce_2/Cu_4Al_1O_x$ is restored to 45.7, 58.7, 72.6 and 85.7%, respectively. Obviously, the $Ce_2/Cu_4Al_1O_x$-LDO shows a much better ability for NO_x activity regeneration.

3.4. Structural and surface physico-chemical properties versus NH_3-SCR activity

The turnover frequency (TOF, s^{-1}) of the SCR reaction would be the most appropriate activity parameter to explain and discuss the effects of the surface chemical structure and composition of the catalysts on their activity performance presented in Figs. 3 and 4 in terms of NO_x conversion. This parameter, however, requires the knowledge of the *chemical nature* of true *active sites* and their *concentration* on the catalyst surface (mol g^{-1}). Such information is not available from the results of the present work. An attempt was made to estimate this TOF parameter based on reported data in the literature on similar to the present catalytic systems. The catalytic activity of pure CeO_2 catalysts with low SSA towards NH_3-SCR (500 ppm NO, NH_3/NO = 1, 5–10 vol% O_2) has been reported [42,43], where low NO_x conversions (< 25%) at temperatures lower than 250 °C were found. Given this information and the present catalytic activity performance results (Fig. 3), we believe it is reasonable to suggest that it is the Cu sites on the present catalytic system that appear to mostly contribute to the high activity observed. Therefore, the TOF (s^{-1}) presented here is defined as the number of NO_x (mols) converted per Cu^{2+} surface (mols) per second, and the respective Eq. 9 is given below:

$$\text{TOF}\,(s^{-1}) = X_{NO_x} F_{NO_x}/(60 \times 22.4 \times \text{amount of } Cu^{2+}) \quad (10)$$

where, F_{NOx} is the feed volume flow rate of NO_x (L/min), X_{NOx} is the NO_x conversion (%), while the amount (mols) of surface Cu^{2+} was calculated using the XPS data. In this TOF (s^{-1}) estimation, it is assumed that the %-Cu on the first atomic layer compared to the total concentration seen in the XPS analysis (few atomic layers from the surface, ca. 3–4 nm) is similar for all the solids examined.

The TOF for NO_x conversion (NH_3-SCR) of the Cu/Al_2O_3 and $Ce_2/Cu_4Al_1O_x$ as a function of reaction temperature is presented in Fig. 6. Apparently, $Ce_2/Cu_4Al_1O_x$-LDO presents significantly higher TOF values than the Cu/Al_2O_3 catalyst in the 100–250 °C range. Therefore, it appears that $Ce_2/Cu_4Al_1O_x$-LDO catalyst contains Cu sites of larger activity (k, s^{-1}), which ultimately lead to higher NO_x conversion values in the whole reaction temperature range investigated. A similar conclusion was obtained by the transient NH_3-SCR kinetics studies to be presented and discussed in Section 3.6.2. In our previous research [44], it was reported that copper in Cu/Al_2O_3 is mainly found as $CuAl_2O_4$ and

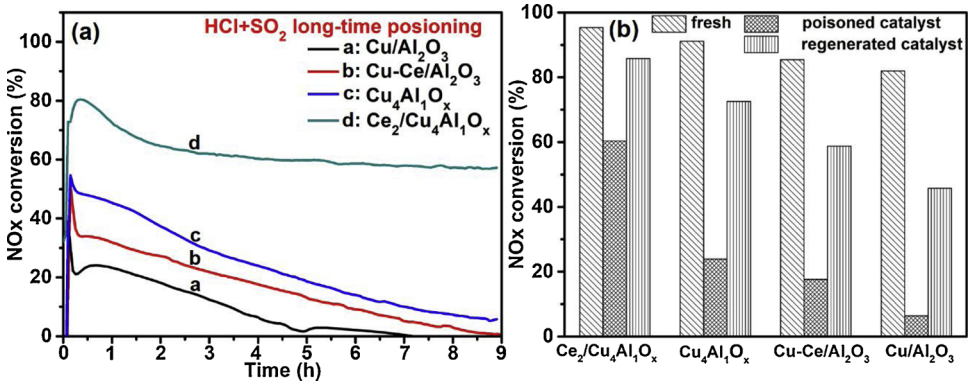

Fig. 5. (a) Stability test of catalysts at 200 °C with 100 ppm HCl and 100 ppm SO_2 in the feed stream, and (b) NO_x conversions of fresh, deactivated and thermally regenerated catalysts. Reaction conditions: $[NO_x] = [NH_3] = 500$ ppm, $[O_2] = 5\%$, $[H_2O] = 5\%$, $[SO_2] = 100$ ppm, [HCl] = 100 ppm, balance Ar, total flow rate = 200 mL/min, GHSV = 60,000 h^{-1}, $W_{cat} = 0.15$ g.

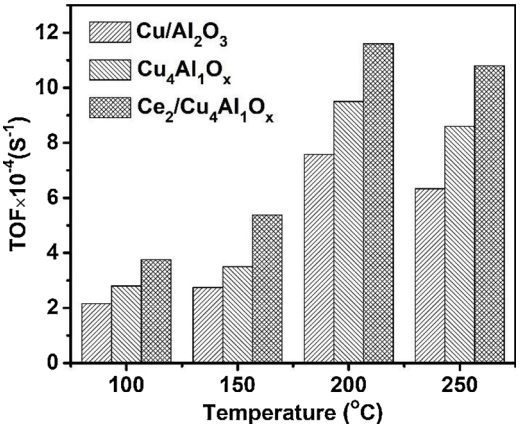

Fig. 6. TOF as a function of temperature profiles of the Cu/Al_2O_3 and $Ce_2/Cu_4Al_1O_x$ – LDO catalysts.

CuO, while in $Ce_2/Cu_4Al_1O_x$-LDO mainly as CuO (Fig. 1b). It was proved that this highly dispersed CuO is more beneficial to improve the NH_3-SCR performance of the catalyst.

The oxidation states of Ce and Cu species in the catalyst samples were investigated by XPS (Fig. 7 and Table 1). Fig. 7a presents Cu 2p XPS spectra of $Ce_2/Cu_4Al_1O_x$, $Cu_4Al_1O_x$, Cu-Ce/Al_2O_3 and Cu/Al_2O_3 catalysts, with two satellite peaks appeared at ~ 937.0–946.0 eV and 959.0–964.0 eV in all samples. The peaks at ~ 933 and 953.0 eV can be assigned to Cu $2p_{3/2}$ and Cu $2p_{1/2}$, respectively [3]. In addition, the surface Cu^{2+} concentration in $Ce_2/Cu_4Al_1O_x$ (87.3%, Table 1) is significantly larger than that in Cu/Al_2O_3 (54.9%), in harmony with its higher catalytic activity. In addition, the Cu^{2+} XPS peak of Cu-Ce/Al_2O_3 is larger and broader, and the $Cu^{2+}/(Cu^{2+}+Cu^{1+})$ atom-% fraction in Cu-Ce/Al_2O_3 (66.9%, Table 1) appears larger than that in Cu/Al_2O_3 (54.9%). It is noted that the peak positions of Cu 2p3/2 in the $Ce_2/Cu_4Al_1O_x$ (~ 933.8 eV) XP spectra slightly shifted towards lower binding energies than those of Cu/Al_2O_3 (~ 933.3 eV), which might be due to the partial charge transfer from Ce to the Cu species. It is thus indicated that introduction of Ce increases the surface concentration of Cu^{2+} species in the Cu-based catalysts examined.

Fig. 7b presents the Ce 3d XPS spectra of $Ce_2/Cu_4Al_1O_x$ and Cu-Ce/Al_2O_3 catalysts. After peak-fitting and deconvolution procedures applied, the Ce 3d peaks are fitted into eight peaks, which agree well with the results reported by Burroughs et al. [45]. The peaks denoted as u (900.4 eV), u" (906.7 eV) and u"' (916.0 eV) belong to $Ce^{4+}3d_{3/2}$, while the peaks denoted as v' (882.0 eV), v" (887.9 eV) and v"' (897.6 eV) belong to $Ce^{4+}3d_{5/2}$. The peak u_0 (902.9 eV) and v_0 (884.9 eV) are attributed to Ce^{3+} [42]. In addition, the surface Ce^{3+} (atom-% fraction) expressed as $Ce^{3+}/(Ce^{3+}+Ce^{4+})$ in the $Ce_2/Cu_4Al_1O_x$ solid (44.7%, Table 1), is apparently higher than that obtained in Cu-Ce/Al_2O_3 (10.5%, Table 1). The surface Ce^{3+} concentration indicates the existence of an equivalent concentration of surface oxygen vacancies [46]. The latter could activate NO_x adsorption intermediates in NH_3-SCR and promote the adsorption of oxygen species [46].

Fig. 7c presents the O 1s XPS spectra of $Ce_2/Cu_4Al_1O_x$, $Cu_4Al_1O_x$, Cu-Ce/Al_2O_3 and Cu/Al_2O_3 catalysts. The peak at ~ 529.7–531.3 eV is related to the lattice oxygen (O_α), whereas the peak at ~ 531.3–532.8 eV to the surface adsorbed oxygen (O_β) [47]. The O_β concentration in $Ce_2/Cu_4Al_1O_x$ catalyst (70%, Table 1) appears to be much higher than that in Cu/Al_2O_3 (57.2%, Table 1). This implies that $Ce_2/Cu_4Al_1O_x$-LDO mixed metal oxide derived after calcination of the corresponding LDH material leads to an enhanced surface concentration of oxygen vacancies since the latter are considered as adsorption sites of O_β. In addition, literature reports have revealed that O_β could facilitate NH_3-SCR due to its higher mobility [48,49]. As reported by Liu et al. [49], O_β could also accelerate the formation of NO_2 via oxidation of NO, thereby promoting the "fast SCR" catalytic reaction.

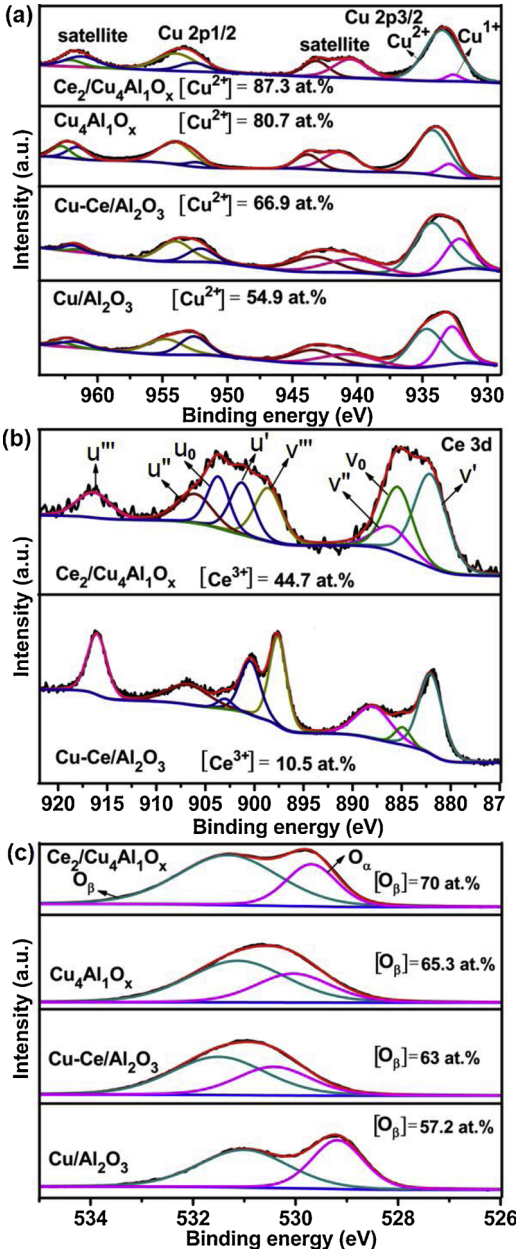

Fig. 7. XPS spectra of (a) Cu 2p, (b) Ce 3d, and (c) O 1s photoelectrons of $Ce_2/Cu_4Al_1O_x$, $Cu_4Al_1O_x$, Cu-Ce/Al_2O_3, and Cu/Al_2O_3 catalysts.

Based on the XPS results (Fig. 7, Table 1), it is suggested that the relatively high concentrations of Cu^{2+}, Ce^{3+} and O_β present in the $Ce_2/Cu_4Al_1O_x$-LDO catalyst, compared to the other Cu/Ce-based catalysts, seem to be responsible for its excellent SCR performance against the other solids in the series investigated. Furthermore, based on the XPS results, a synergistic interaction between Cu and Ce might exist according to the redox couple: $Ce^{3+} + Cu^{2+} \leftrightarrow Ce^{4+} + Cu^{+}$ [50]. It is suggested that the redox ability of Cu species in the ternary mixed metal oxide is significantly enhanced by the addition of Ce, compared to Cu-Al-O, which in turn, the electron-rich Cu sites (Cu^{+}) promote NO_x conversion activity.

The surface acidity of the investigated solid catalysts was evaluated using pyridine (Py)-FTIR and results are shown in Fig. 8a for the $Ce_2/Cu_4Al_1O_x$, $Cu_4Al_1O_x$, Cu-Ce/Al_2O_3 and Cu/Al_2O_3 catalysts. The absorption IR bands that appear at ~ 1442, 1489, 1575 and 1608 cm^{-1} are ascribed to coordinated pyridine species to the Lewis (L) surface acid sites, whereas the characteristic IR band attributed to Brönsted (B)

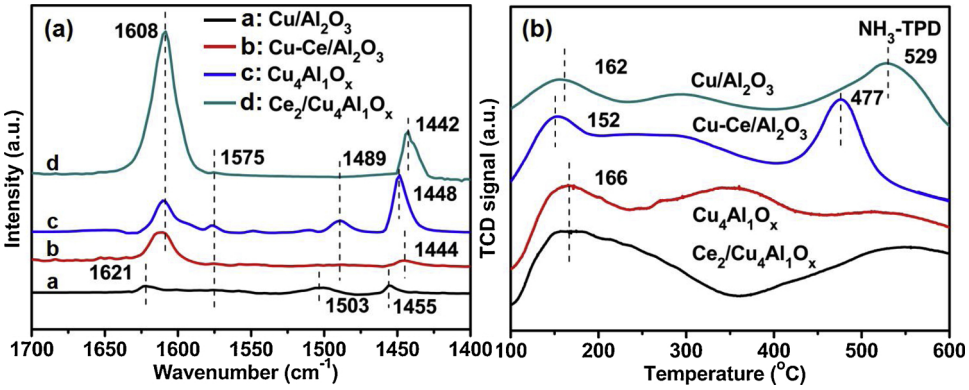

Fig. 8. (a) FTIR spectra of pyridine adsorbed at 200 °C on the surface of catalysts; (b) NH_3-TPD traces of catalysts.

surface acid sites appears as a weak IR band (1523 cm^{-1}, $Cu_4Al_1O_x$, Fig. 8a) [51]. It was found that the amount of Lewis acid sites decreases in the order: $Ce_2/Cu_4Al_1O_x$ (747.7 μmol/g) > $Cu_4Al_1O_x$ (301.4 μmol/g) > Cu-Ce/Al_2O_3 (139.8 μmol/g) > Cu/Al_2O_3 (49.7 μmol/g). Obviously, after the introduction of Ce, the amount of Lewis surface acid sites is increased, which could partly explain the improved de-NO_x performance of $Ce_2/Cu_4Al_1O_x$-LDO catalyst. Peña et al. [52] indicated that the main active sites in NH_3-SCR might be attributed to the Lewis surface acid sites, while Brönsted acid sites have less influence on the NH_3-SCR of NO_x. Yang et al. [53] indicated that the coordinated NH_3 species formed on the L surface acid sites is further dehydrogenated to form an intermediate amide species (−NH_2), which is highly reactive. In addition, L acid sites are considered as very important surface active sites in the NH_3-SCR [54,55].

NH_3-TPD traces over the same catalysts are presented in Fig. 8b. Two main ammonia desorption peaks for the Cu-Ce/Al_2O_3, Cu/Al_2O_3 and $Ce_y/Cu_4Al_1O_x$ solids are observed, which are attributed to chemisorption on Ce and Cu cationic Lewis surface acid sites but also to the −OH species (Brönsted acid sites). The first low-temperature main desorption peak appears in the 152–166 °C range with shoulder on its falling part. The second high-temperature desorption peak is observed at T > 400 °C (e.g. 477 and 529 °C, Fig. 8b). A third discernable small ammonia desorption peak is clearly observed over $Cu_4Al_1O_x$ at temperatures in the 250–450 °C range (Fig. 8b). The amount of surface acid sites of $Ce_2/Cu_4Al_1O_x$, $Cu_4Al_1O_x$, Cu-Ce/Al_2O_3 and Cu/Al_2O_3 catalysts can be estimated after integrating the TPD curves. This was found to be in line with the pyridine FTIR results, where the surface acidity of $Ce_2/Cu_4Al_1O_x$ is much higher than that of $Cu_4Al_1O_x$, Cu-Ce/Al_2O_3 and Cu/Al_2O_3 solids.

3.5. HCl and SO_2 activity poisoning effects

According to the literature [40], the poisoning effect of HCl over Ce-Sn-Ti-O mixed metal oxides in NH_3-SCR is mainly due to the formation of metal chlorides by the interaction between active metal species (e.g., Cu^{2+}, Ce^{3+}/Ce^{4+}) and Cl^-, which would normally lead to the decline of redox behavior of active metal species. In this work, we also examined the redox performance of catalysts before and after pre-chlorination treatment using H_2 temperature-programmed reduction (H_2-TPR) analyses and the obtained results are presented in Fig. 9. The pre-chlorination treatment was performed by exposing the catalysts to 500 ppm HCl for 3 h (see also Section 2.2). It is shown that reduction peak temperatures for the pre-chlorinated catalysts are all shifted to higher temperatures, indicating that HCl has a negative influence on the reducibility of NH_3-SCR catalysts. In particular, for the Cu/Al_2O_3 and Cu-Ce/Al_2O_3 catalysts, two H_2 reduction peaks appear (Fig. 9b). According to the literature [50], the low temperature (ca. 252 and 287 °C) H_2 reduction peak is associated with the reduction of CuO species ($Cu^{2+} \rightarrow Cu^{1+} \rightarrow Cu^0$), whereas the 2nd reduction peak observed at high temperatures (ca. 496 and 472 °C) is associated with the reduction of Cu^{2+} and/or Ce^{4+} present in the bulk of their respective oxide. In the case of Cu/Al_2O_3, the two reduction peaks (ca. 287 and 472 °C) attributed to Cu species are largely shifted to 385 and 565 °C after pre-chlorination (Fig. 9b). On the other hand, in the case of $Ce_2/Cu_4Al_1O_x$-LDO, the low-temperature reduction peak (Fig. 9a) after pre-chlorination treatment is only slightly shifted, namely from 205 to 281 °C. Compared with Cu/Al_2O_3 and Cu-Ce/Al_2O_3 (Fig. 9b) catalysts, the low-temperature reduction peak of $Ce_2/Cu_4Al_1O_x$ appears larger, and the H_2 reduction peak temperature is significantly shifted to lower temperatures. This result could partly explain the best HCl resistance of $Ce_2/Cu_4Al_1O_x$ observed compared to all the other catalysts investigated. Furthermore, with the introduction of Ce, the peak temperature attributed to the reduction of Cu species shifts to lower temperatures, indicating that the reducing ability of oxidized Cu species is affected by its interaction with Ce.

After the pre-chlorination treatment, the amount of deposited Cl on the Cu/Al_2O_3, Cu-Ce/Al_2O_3, $Cu_4Al_1O_x$ and $Ce_2/Cu_4Al_1O_x$ catalysts was estimated using ion chromatography (ICS). Table 1 shows that the Cl content in $Ce_2/Cu_4Al_1O_x$ (0.56 mg/g) is much less than that in $Cu_4Al_1O_x$ (0.76 mg/g), Cu-Ce/Al_2O_3 (0.99 mg/g) and Cu/Al_2O_3 (1.81 mg/g). Therefore, ICS and H_2-TPR analyses suggest that the least amount of Cl species was deposited on $Ce_2/Cu_4Al_1O_x$-LDO, result that is in harmony with its better HCl-resistance performance obtained (Figs. 4 and 5). Yang et al. [56] reported that the addition of Cl not only inhibited adsorption of NH_3 but also that of NO_x species, leading to the deactivation of catalyst. The alleviation of Cl deposition on $Ce_2/Cu_4Al_1O_x$ catalyst might be attributed to the increased concentration of its surface acid sites, the catalyst's redox properties, and the higher dispersion of active Cu species and of Ce-promoting species of catalyst activity, as previously mentioned.

In situ DRIFTS studies were conducted to gain more fundamental information about the nature of NO_x adsorption sites that are poisoned by the presence of SO_2 in the NH_3-SCR reaction. A 2000 ppm NO/5% O_2/Ar adsorption gas mixture was first conducted for 30 min at 200 °C. Fig. 10a–d show the FTIR spectra recorded as a function of time for the four catalysts indicated. The IR bands located at ~ 1606–1608, 1545–1551 and 1277–1280 cm^{-1} appear in all catalysts. According to the literature [57,58], the IR band located at 1606–1608 cm^{-1} is attributed to the adsorption of NO_2 in the bidentate form of nitrate, the IR band located at 1545–1551 cm^{-1} to bidentate nitrates (e. g. NO_3 and nitrito (O-bound NO_2) species) [59], and the IR band at 1277–1280 cm^{-1} is attributed to monodentate nitrate species [57,60]. These results tend to suggest that after the introduction of Ce in the Cu−Al−O solid, the oxidation of NO to NO_2 might occur at low temperatures. It was reported [61] that the presence of NO_2 facilitates the formation of ammonium nitrite (NH_4NO_2) and accelerates the "fast SCR".

After the introduction of SO_2 in the NO/O_2/Ar gas mixture, the IR

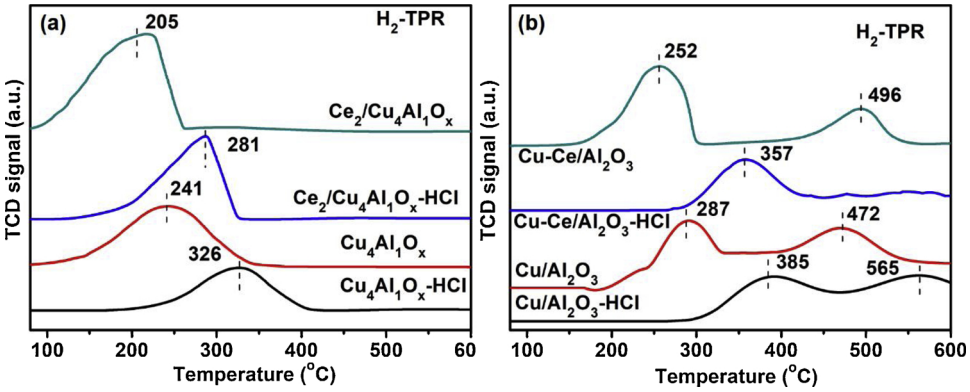

Fig. 9. H_2-TPR traces of fresh and pre-chlorinated $Ce_2/Cu_4Al_1O_x$ and $Cu_4Al_1O_x$ catalysts (a) and of fresh and pre-chlorinated Cu-Ce/Al_2O_3 and Cu/Al_2O_3 catalysts (b).

bands attributed to adsorbed NO_x species disappear (Fig. 10), except the IR band located at 1606–1608 cm^{-1}, where at the same time a new IR band located at 1340–1354 cm^{-1} appears, which is due to the asymmetric stretching vibrational mode of O═S═O [62]. These results strongly suggest the strong competitive nature of SO_2 and NO_x chemisorption for the same surface adsorption sites, leading to the decrease in the amount of NO_x adsorption. Notably, the intensity of the IR band attributed to sulfur species on the $Ce_2/Cu_4Al_1O_x$ surface appears significantly weaker compared to the other catalysts, whereas IR bands of NO_x species on the $Ce_2/Cu_4Al_1O_x$ catalyst appear stronger than those in the other catalysts. These results further prove that $Ce_2/Cu_4Al_1O_x$ catalyst has superior SO_2 tolerance.

In order to evaluate the effect of SO_2 on ammonia chemisorption, similar in-situ DRIFTS studies performed with the $NO/O_2/Ar$ gas treatment, were also conducted at 200 °C for the NH_3/N_2 gas treatment. Fig. 11 shows in-situ DRIFTS spectra recorded on Cu/Al_2O_3, Cu-Ce/Al_2O_3, $Cu_4Al_1O_x$ and $Ce_2/Cu_4Al_1O_x$ catalysts under flowing 1000 ppm NH_3/N_2 and under a gas mixture containing in addition 500 ppm SO_2 for different adsorption times. The IR bands that appear at 1596–1602 cm^{-1} and 1179–1191 cm^{-1} are attributed to the chemisorption of NH_3 on Lewis (L) surface acid sites [43,63], whereas the IR bands at 1672–1680 cm^{-1} and 1437–1446 cm^{-1} can be assigned to NH_4^+ species on the Brönsted (B) surface acid sites [64,65]. It is clearly seen that the intensities of the IR bands appeared at 1598 and 1676 cm^{-1} in the $Ce_2/Cu_4Al_1O_x$ catalyst are stronger compared to those in the other catalysts, suggesting that the presence of Ce in the catalyst composition can largely enhance adsorption of NH_3. The NH_3-DRIFTS results agree well with those of Py-FTIR (Fig. 8a) and NH_3-TPD (Fig. 8b), where the enhanced concentration of L and B surface acid sites formed on $Ce_2/Cu_4Al_1O_x$-LDO correlates with its higher catalytic activity (Fig. 3).

Following the gas treatment of the catalysts for 30 min in the $NH_3/$

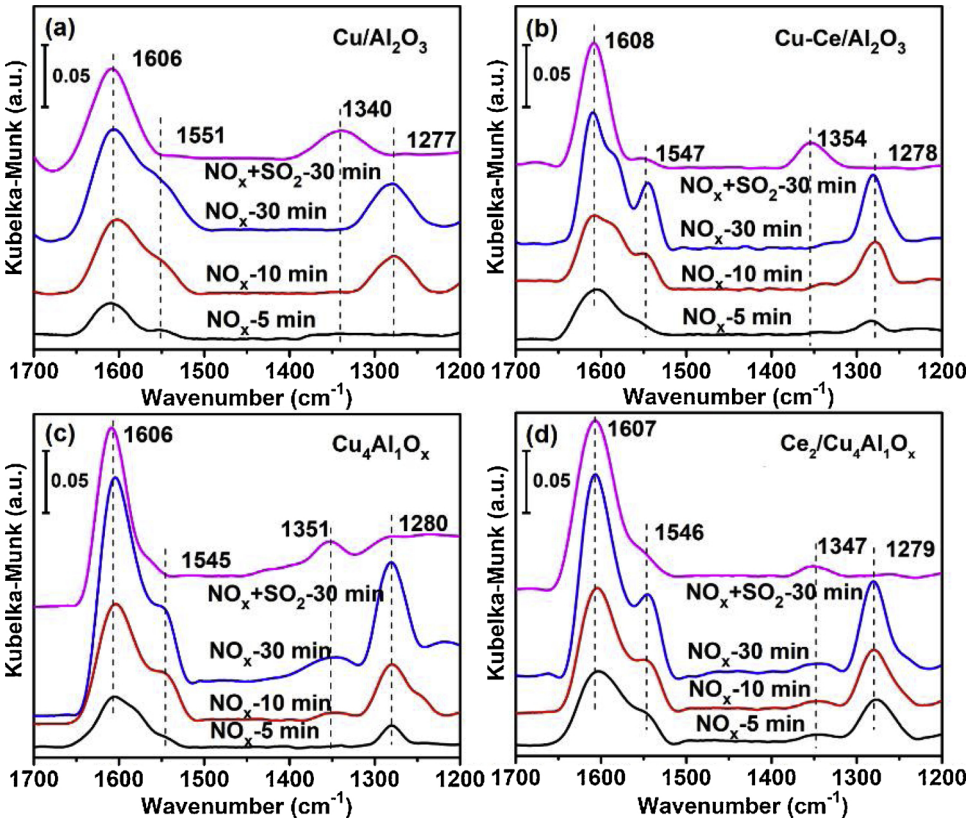

Fig. 10. *In situ* DRIFTS spectra obtained after a 30-min exposure of catalysts at 200 °C to 2000 ppm NO + 5% O_2 or 2000 ppm NO + 500 ppm SO_2 in the presence of 5% O_2 over (a) Cu/Al_2O_3, (b) Cu-Ce/Al_2O_3, (c) $Cu_4Al_1O_x$ and (d) $Ce_2/Cu_4Al_1O_x$ catalysts.

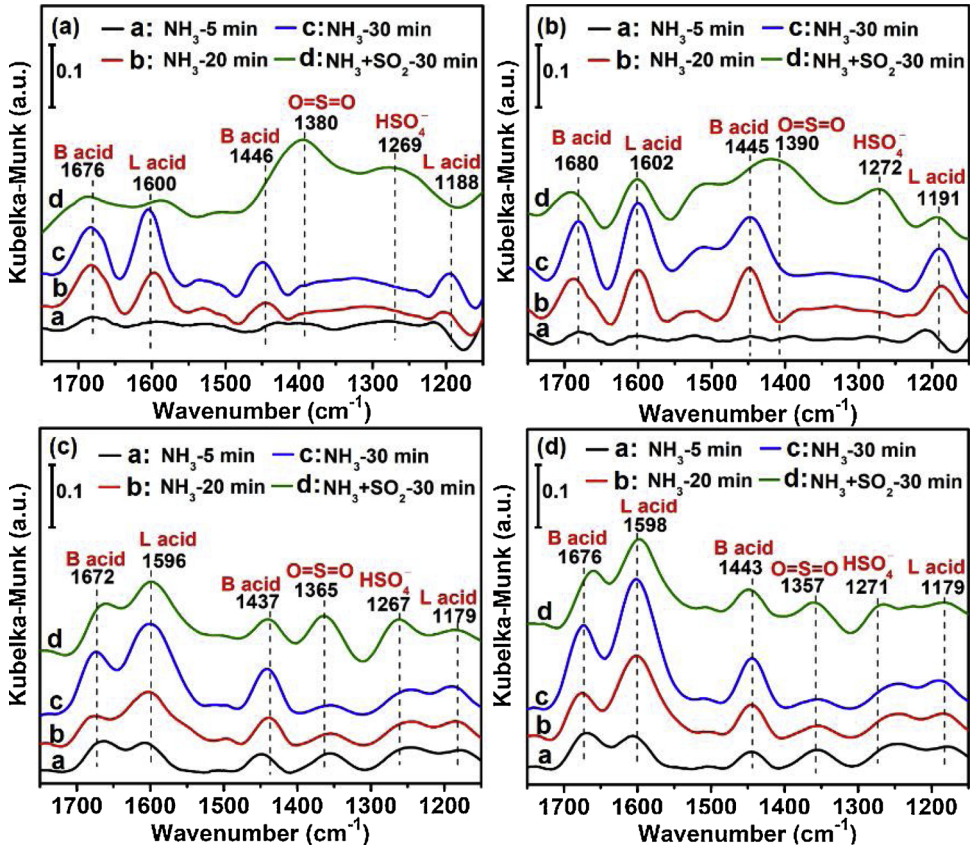

Fig. 11. *In situ* DRIFTS spectra obtained after a 30-min exposure of catalysts at 200 °C to 1000 ppm NH_3 or 1000 ppm NH_3 + 500 ppm SO_2 in the presence of 5% O_2 over (a) Cu/Al_2O_3, (b) $Cu\text{-}Ce/Al_2O_3$, (c) $Cu_4Al_1O_x$ and (d) $Ce_2/Cu_4Al_1O_x$ catalysts.

SO_2/N_2 gas mixture, the intensity of the IR band attributed to NH_3 chemisorption on the L surface acid sites (1596–1600 cm^{-1}) and that of NH_4^+ on the B surface acid sites (1672–1680 cm^{-1}) are found to decrease. This suggests that the amount of surface acid sites on the catalyst is reduced. It should be noted that new IR bands at 1357–1390 cm^{-1} and 1267–1272 cm^{-1} appear, and these are attributed to O═S═O and HSO_4^- species, respectively [62]. It is shown that NH_3 adsorption is indeed affected by the presence of SO_2, the result of which is the formation of NH_4HSO_4 or $(NH_4)_2SO_4$ species. It is worth noting that $Ce_2/Cu_4Al_1O_x$ catalyst in the co-presence of SO_2 and NH_3 has shown a relatively larger concentration of surface acid sites and less $(NH_4)_2SO_4$ or NH_4HSO_4, which is likely related to the superior activity and stability of this catalyst composition.

In addition to the above mentioned, the deposited S and Cl on the pre-poisoned and regenerated $Ce_2/Cu_4Al_1O_x$ and $Cu\text{-}Ce/Al_2O_3$ catalysts were evaluated by SEM-EDS analyses, and results are presented in Figs. S4 and S5. After the applied pre-sulfidation and pre-chlorination treatments, the amounts of S and Cl species deposited on the surface of $Ce_2/Cu_4Al_1O_x$ catalyst were found to be 3.6 and 1.1 wt%, respectively, lower than that on $Cu\text{-}Ce/Al_2O_3$ (4.0 wt% for S and 2.0 wt% for Cl). Both amounts of S and Cl species were decreased after regeneration, but it seems difficult to completely decompose the metal sulfates and metal chlorides formed. For the regenerated $Ce_2/Cu_4Al_1O_x$ catalyst, the S and Cl species deposited decreased to 2.5 wt% and 0.5 wt%, respectively, which are lower than those on $Cu\text{-}Ce/Al_2O_3$ (3.65 wt% for S and 0.71 wt% for Cl). The SEM-EDS results indicated that the sulfate and chloride species indeed existed on the surface of catalysts, although their amounts were very small, and that the $Ce_2/Cu_4Al_1O_x$ catalyst had the best resistance to SO_2 and HCl.

In this study, Cu^+ and Cu^{2+} were detected in the $Ce_2/Cu_4Al_1O_x$ catalyst by H_2-TPR and XPS analyses. It was shown that Cu^{2+} is partially reduced to Cu^+ with the introduction of Ce in the catalyst composition, which further indicates that a strong synergistic interaction between copper and cerium species can take place, namely: $Ce^{3+} + Cu^{2+} \leftrightarrow Ce^{4+} + Cu^+$ [50]. The synergistic effect between copper and cerium species is considered to largely promote the SCR process according to Scheme 1. It is also suggested that NO could be oxidized in the presence of O_2 to NO_2 during SCR. It was reported [58,66] that both E-R and L-H mechanisms could operate in the NH_3-SCR reaction process on $CeO_2\text{-}WO_3/TiO_2$. According to these mechanisms, gaseous NH_3 is adsorbed on Lewis acid sites to form coordinated NH_3 and/or is adsorbed also on the Brönsted acid sites to form NH_4^+. The latter species could then interact with adsorbed NO_x (L-H mechanism) and/or gaseous NO (E-R mechanism). A comparison of the relative activity of adsorbed NH_3 with NO/O_2 on the best $Ce_2/Cu_4Al_1O_x$ and one of the worst $Cu\text{-}Ce/Al_2O_3$ catalysts observed in this work is presented in the following Section 3.6.2 via transient kinetics studies. These studies support the view that both L-H and E-R mechanisms seem to operate on the present $Ce_2/Cu_4Al_1O_x$-LDO catalyst and the latter better promotes NO oxidation to NO_2.

3.6. Transient kinetics studies

3.6.1. Transient NH_3 chemisorption

To elucidate some intrinsic kinetic reasons for the superior NH_3-SCR performance of $Ce_2/Cu_4Al_1O_x$-LDO compared to the $Cu\text{-}Ce/Al_2O_3$ catalyst reported in Fig. 3, we have designed and performed transient kinetics experiments to estimate: (i) the rate evolution of NH_3 chemisorption and the maximum surface concentration of adsorbed ammonia species obtained under 1000 ppm NH_3/He gas flow at 150 and 200 °C, (ii) the transient evolution of N_2 and N_2O formation rates due to the reaction of pre-adsorbed ammonia with NO in the presence of O_2 upon the gas switch NH_3/He → NO/O_2/He (t) at the same T (150 or 200 °C), details of which are given in Section 2.4, (iii) the amount of adsorbed

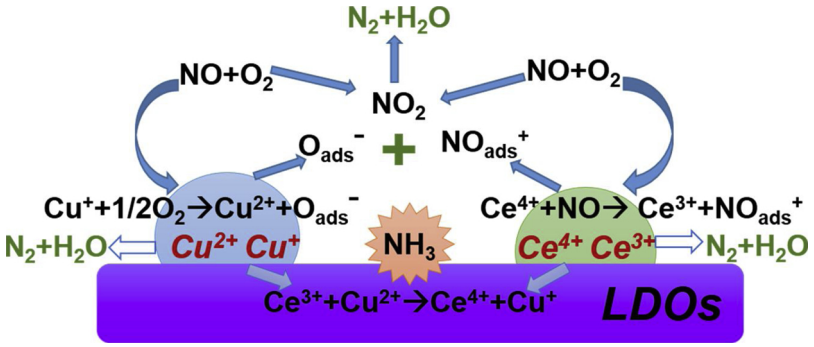

Scheme 1. Schematic illustration of the redox catalytic cycle of the low-temperature NH_3-SCR of NO_x over $Ce_y/Cu_4Al_1O_x$ - LDO catalysts.

NO_x-s after completion of the transient NH_3-SCR, (iv) the rate evolution of NO chemisorption towards NO_x adsorbed species and the formation of N_2O/NO_2 in the presence or absence of gaseous oxygen, and (v) the reactivity of adsorbed NO_x-s towards 5%O_2/He gas mixture at 150 °C. The results obtained from these transient kinetics studies are presented in what follows.

Fig. 12A and B show comparative specific transient rates (μmol $m^{-2} s^{-1}$) of ammonia chemisorption at 150 and 200 °C, respectively, over the two catalysts; these specific rates were estimated after using Eq. (3) and the SSA ($m^2 g^{-1}$) of the solids. It should be noted that no other gases (e.g. N_2, N_2O, NO or NO_2) were measured by mass spectrometry during this transient adsorption experiment. It is seen that ammonia chemisorption over Cu-Ce/Al_2O_3 at 150 and 200 °C reaches saturation (under 1000 ppm NH_3/He) within ~ 20 and 15 min,

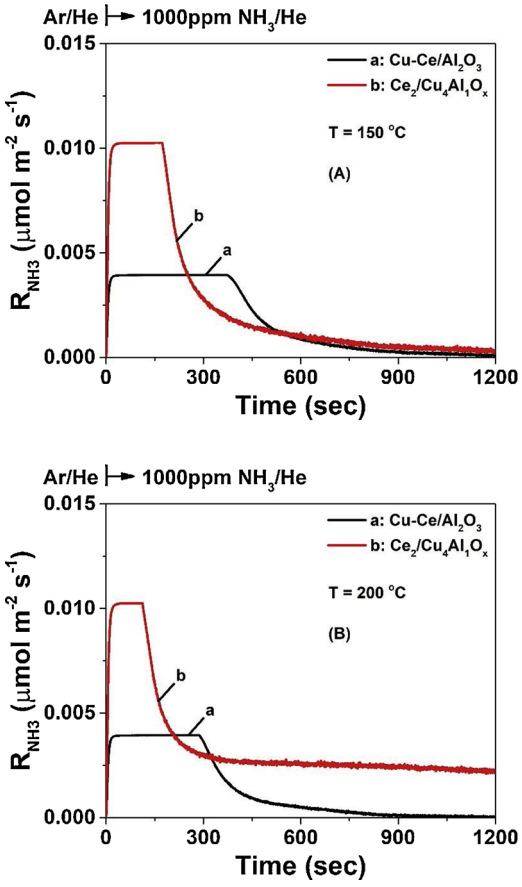

Fig. 12. Transient rates (μmol $m^{-2} s^{-1}$) of NH_3 chemisorption as a function of time estimated via Eq. (3) after the gas switch Ar/He → 1000 ppm NH_3/1%Kr/He (t) at 150 (A) and 200 °C (B) over a: Cu-Ce/Al_2O_3 and b: $Ce_2/Cu_4Al_1O_x$ catalysts; F_T = 50 N mL min^{-1}; W_{cat} = 0.05 g.

respectively, and this corresponds to an adsorbed amount of 284.5 and 212.5 μmol NH_3 g^{-1}, respectively. These results imply for a non-activated NH_3 chemisorption process. On the other hand, the $Ce_2/Cu_4Al_1O_x$ solid shows significantly larger initial adsorption rates of ammonia than Cu-Ce/Al_2O_3 at 150 °C (Fig. 12A) and also a larger NH_3 saturation amount, ca. 363.5 μmol g^{-1}. After increasing the adsorption T to 200 °C (Fig. 12B), the $Ce_2/Cu_4Al_1O_x$ solid continues to adsorb ammonia even after 20 min of time on stream, where NH_3 adsorption on Cu-Ce/Al_2O_3 has already been completed. This result corresponds to a larger than 285 μmol NH_3 g^{-1}; the latter amount is for 20 min of adsorption. It is also seen that during the period of 5–20 min on stream, the rate of NH_3 chemisorption decreases only slightly, as opposed to the case of lower T (150 °C, Fig. 12A). These results are very important and informative, suggesting that $Ce_2/Cu_4Al_1O_x$ likely possesses two kinds of acidic sites, one with a large heat of adsorption, which is filled first, and another one which is filled slowly but likely of a larger concentration. Ammonia chemisorption on this site is likely to be associated with an activation barrier. The latter finds support by the fact that this slow rate of ammonia chemisorption becomes even slower at 150 °C (compare rates of chemisorption after 5 min on stream). Furthermore, the concentration of such activated ammonia chemisorption sites appears larger compared to that of the strong acid sites, for which the initial chemisorption period is due to. The transient ammonia chemisorption results are in harmony with the NH_3-TPDs reported in Fig. 8b, where the amount of weakly chemisorbed ammonia (desorption in the 100–350 °C range) is larger for $Ce_2/Cu_4Al_1O_x$ than Cu-Ce/Al_2O_3 solid. Furthermore, the saturation amount of adsorbed ammonia (1000 ppm NH_3/He) at both 150 and 200 °C is significantly larger on $Ce_2/Cu_4Al_1O_x$ than Cu-Ce/Al_2O_3, in agreement with the pyridine FTIR adsorption measurements (Fig. 8a). The fact that most of the weakly chemisorbed ammonia over the two solids presents similar binding strength (T_M = 162–166 °C, Fig. 8b), the higher rates of ammonia chemisorption per m^2 observed on $Ce_2/Cu_4Al_1O_x$ are due to its larger density of acidic sites compared to the case of Cu-Ce/Al_2O_3. In fact, the Py-FTIR (Fig. 8a) and in situ DRIFTS (Fig. 11) of ammonia reveal that the $Ce_2/Cu_4Al_1O_x$ catalyst possesses larger amount of acid sites than the other catalysts, which is in line with the higher initial rate of ammonia chemisorption compared to Cu-Ce/Al_2O_3 catalyst. It should also be noted that the initial plateau in the rate of ammonia chemisorption (Fig. 12A, B) is because during this short period, all NH_3 fed into the micro-reactor is chemisorbed.

3.6.2. *Transient NH_3-SCR*

Fig. 13A and B show the specific transient rates of NO consumption (μmols NO $m^{-2} s^{-1}$) (Eq. (7)) as the result of reaction with NH_3-s (pre-adsorbed ammonia) upon the switch 1000 ppm NH_3/Ar/He → 1000 ppm NO/5% O_2/Ar/Kr/He at 150 and 200 °C, respectively, over the two catalysts. It is clearly seen that the rates of NO consumption at the initial transient (ca. 5 min on stream) are always larger in the case of $Ce_2/Cu_4Al_1O_x$ at both reaction temperatures. There is a long tail after about 5 min of reaction (up to 20 min on stream), especially for the $Ce_2/Cu_4Al_1O_x$ catalyst, which is due both to the adsorption of NO to form

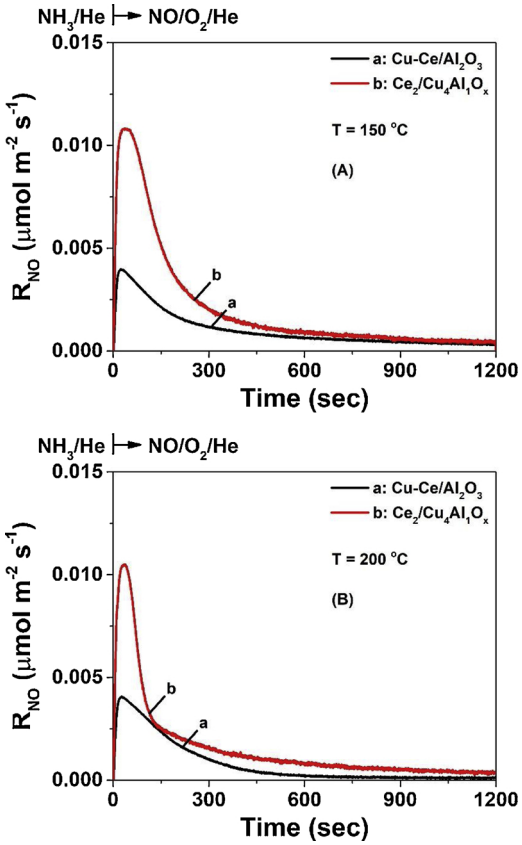

Fig. 13. Transient rates (μmol $m^{-2} s^{-1}$) of NO consumption as a function of time estimated via Eq. (7) after the gas switch 1000 ppm NH_3/He (20 min) → 1000 ppm NO/5% O_2/1% Kr/Ar/He (t) at T = 150 °C (A) and T = 200 °C (B) over a: Cu-Ce/Al_2O_3 and b: $Ce_2/Cu_4Al_1O_x$ catalysts; F_T = 50 N mL min^{-1}; W_{cat} = 0.05 g.

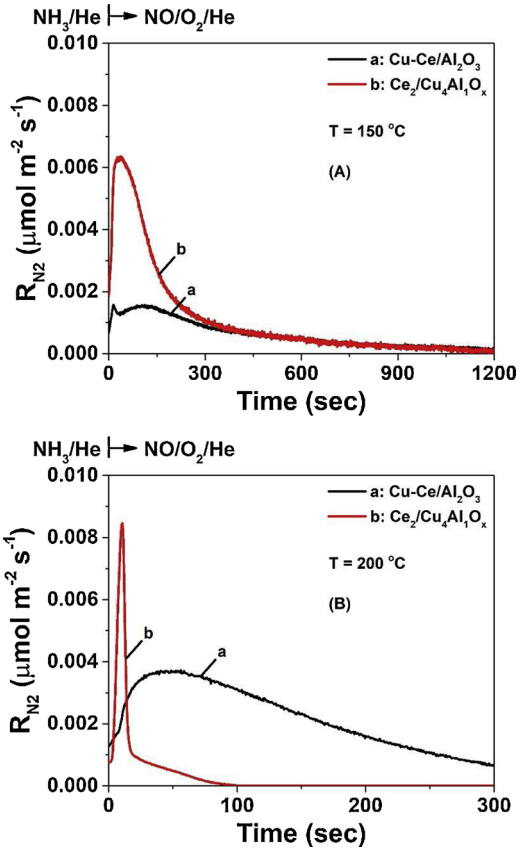

Fig. 14. Transient rates (μmol $m^{-2} s^{-1}$) of N_2 production as a function of time estimated via Eq. (8) after the gas switch 1000 ppm NH_3/He (20 min) → 1000 ppm NO/5% O_2/1% Kr/Ar/He (t) at T = 150 °C (A) and T = 200 °C (B) over a: Cu-Ce/Al_2O_3 and b: $Ce_2/Cu_4Al_1O_x$ catalysts; F_T = 50 N mL min^{-1}; W_{cat} = 0.05 g.

various kinds of NO_x-s but also to the slow reduction of a small amount of pre-adsorbed ammonia at the lowest T of 150 °C. This explanation for the observed tail in the transient curve of NO consumption rate is related to the corresponding transient rates of N_2 gas formation depicted in Fig. 14A and B. It is illustrated that at T = 150 °C, there is a tail of N_2 formation, while this is absent in the case of higher temperature, T = 200 °C (Fig. 14B). In the latter case, it is shown that the initial rate of N_2 formation is ~ 7 times larger on $Ce_2/Cu_4Al_1O_x$ compared to Cu-Ce/Al_2O_3, and the transient reaction of pre-adsorbed NH_3-s species with NO/O_2 lasts only ~ 100 s, as opposed to the significantly larger time needed in the case of Cu-Ce/Al_2O_3 catalyst (larger than 300 s, Fig. 14b). For the latter, a broad N_2 response curve is obtained as opposed to the $Ce_2/Cu_4Al_1O_x$ catalyst. According to Table 2, the amount of N_2 formed after 20 min in NO/O_2/He feed gas stream is larger in the case of $Ce_2/Cu_4Al_1O_x$ compared to Cu-Ce/Al_2O_3 catalyst. These results strongly suggest that the reactivity of sites (k, s^{-1}) responsible for the chemisorption of NH_3-s species towards NO must be significantly larger for $Ce_2/Cu_4Al_1O_x$ compared to Cu-Ce/Al_2O_3 catalyst. In fact, the initial amount of chemisorbed ammonia before the switch to NO/O_2/He is larger on the former than the latter catalyst.

Considering the time at which maximum rates of NO consumption (Fig. 13) and N_2 formation (Fig. 14) are obtained, and the stoichiometry of NH_3-SCR ($R_{NO} = R_{N2}$), it can be verified that the rate of NO consumption is larger than that of N_2 formation, which implies that NO is adsorbed on the catalyst surface during reaction with preadsorbed NH_3-s species. It is important at this point to emphasize that this transient NH_3-SCR experiment (Figs. 13 and 14) allows to estimate the amount (μmol g^{-1}) of chemisorbed NO_x-ads at T = 150 and 200 °C on a surface that is first covered by NH_x-s, thus under conditions closer to the steady-state NH_3-SCR than to an initially clean catalyst surface. This amount should be appreciated as the closest to steady-state NH_3-SCR than that usually estimated and reported from NO-TPD experiments. This NO_x-ads amount is reported in Table 2 along with the amount of NO consumed, N_2 and N_2O produced, which are all estimated after applying Eqs. (4), (7) and (8).

It is seen that at T = 150 °C, the $Ce_2/Cu_4Al_1O_x$ catalyst can accommodate 77.0 μmol g^{-1} NO_x-ads, which is ~ 43% larger than that on the Cu-Ce/Al_2O_3 catalyst. On the other hand, at T = 200 °C, Cu-Ce/Al_2O_3 presents larger amounts of NO_x-ads by ~ 42% compared to the $Ce_2/Cu_4Al_1O_x$ catalyst (Table 2). This result must be related to the relative concentration (mol g^{-1}) of NO_x adsorption sites available in each catalyst sample but also to the relative strength of NO_x-s adsorbed species formed with the surface under the NO/O_2 gas mixture. In fact, as will be shown in the following Section 3.6.3, Cu-Ce/Al_2O_3 is able to form a significantly larger concentration of NO_x-ads under 1000 ppm NO/5%O_2/He than the $Ce_2/Cu_4Al_1O_x$ catalyst.

The obtained quantitative results reported in Table 2 can be used to better understand the NO_x conversion vs T profiles shown in Fig. 3a. At 150 °C, it is seen that $Ce_2/Cu_4Al_1O_x$ catalyst (most active) exhibits a larger amount of active NO_x by ~ 18%, compared to Cu-Ce/Al_2O_3 (compare the sum of N_2 and N_2O formed). However, the difference in NO_x conversion is more than twice (Fig. 3). These results suggest that the site activity (k, s^{-1}) of active NH_x-s (ammonia related active surface intermediates) leading mainly to N_2 must be significantly larger in $Ce_2/Cu_4Al_1O_x$ than Cu-Ce/Al_2O_3 catalyst. At 200 °C, the difference in NO_x conversion becomes small (Fig. 3), but still $Ce_2/Cu_4Al_1O_x$ shows even larger concentration of active NH_x-s than Cu-Ce/Al_2O_3. It appears that as the reaction temperature increases, the difference in reactivity of

Table 2
Amounts (μmol g^{-1}) of NO consumed, NH_3 desorbed, N_2 and N_2O produced as well as of adsorbed NO_x-s for the $Ce_2/Cu_4Al_1O_x$ – LDO and Cu-Ce/Al_2O_3 catalysts at T = 150 and 200 °C following the gas switch: 1000 ppm NH_3/He (20 min) → 1000 ppm NO/5% O_2/1% Kr/Ar/He (T, t).

Catalyst	NO_{cons} (μmol g^{-1})	NH_3 (μmol g^{-1})	N_2 (μmol g^{-1})	N_2O (μmol g^{-1})	NO_x-ads = $NO_{cons} - (N_2 + N_2O)$ (μmol g^{-1})	S_{N2} (%) = $(N_2/(N_2 + N_2O)) \times 100$
$Ce_2/Cu_4Al_1O_x$ -150 °C	209.8	122.8	129.1	3.7	77.0	97.2
$Ce_2/Cu_4Al_1O_x$ -200 °C	162.9	91.2	120.1	2.4	40.4	98.1
Cu-Ce/Al_2O_3 -150 °C	166.0	105.9	87.9	24.6	53.5	78.1
Cu-Ce/Al_2O_3 -200 °C	124.4	62.5	42.8	12.2	69.4	77.7

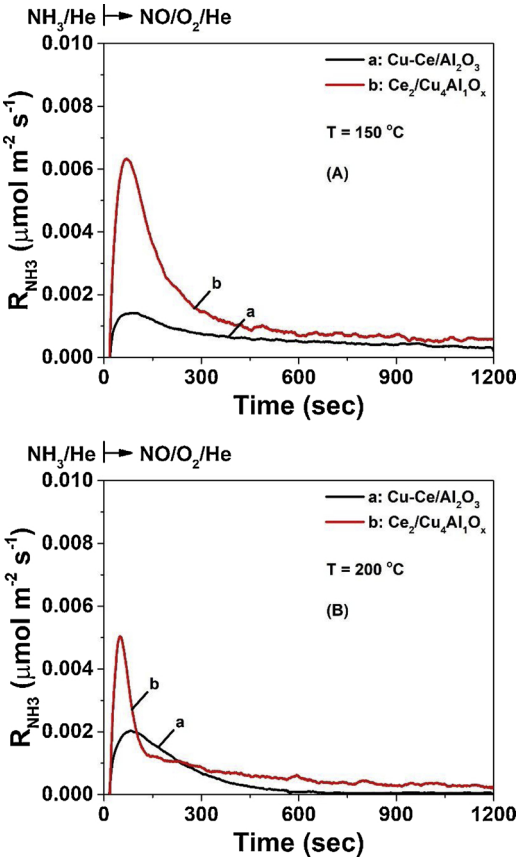

Fig. 15. Transient rates (μmol m^{-2} s^{-1}) of NH_3 desorption as a function of time estimated via Eq. (8) after the gas switch 1000 ppm NH_3/He (20 min) → 1000 ppm NO/5% O_2/1% Kr/Ar/He (t) at T = 150 °C (A) and T = 200 °C (B) over a: Cu-Ce/Al_2O_3 and b: $Ce_2/Cu_4Al_1O_x$ catalysts; F_T = 50 N mL min^{-1}; W_{cat} = 0.05 g.

adsorbed NH_x-s becomes likely more important than the surface coverage of NH_x-s. This result might be related to the chemisorption behavior of NH_3 at 200 °C over the $Ce_2/Cu_4Al_1O_x$ catalyst (Fig. 12B), where a large amount of adsorbed ammonia is accommodated with a slow rate, likely less reactive than the first kind of adsorbed ammonia, as discussed in the previous Section 3.6.1.

An average N_2-selectivity for the transient NH_3-SCR can also be estimated, based on the amounts of N_2 and N_2O formation, which is reported in Table 2 for the two catalysts and temperatures investigated. It is illustrated that this average N_2-selctivity is higher than 97% for $Ce_2/Cu_4Al_1O_x$ as opposed to the lower values obtained for the Cu-Ce/Al_2O_3 catalyst (78%), in harmony with the steady-state NH_3-SCR values reported in Fig. 3c.

Fig. 15 shows the transient rates of ammonia desorption during the NO/O_2/He gas switch over the catalysts at T = 150 (A) and 200 °C (B). It is seen that upon the switch to the reactive gas of 1000 ppm NO/5% O_2/He, ammonia desorbs since part of it, which was reversibly chemisorbed (under NH_3/He), is not able to react and desorbs into the gas phase. Based on the shape of these ammonia isothermal transient desorption rates, weekly adsorbed NH_3-s shows similar desorption and reaction rates towards NO/O_2 at the initial stage of the transient, while as time of reaction goes by lower desorption rates are obtained. The amount of ammonia desorbed under the 20-min treatment of the catalysts with NO/O_2/He was estimated via Eq. (8), and this is reported in Table 2. It is seen that $Ce_2/Cu_4Al_1O_x$ desorbs larger amounts of NH_3 than Cu-Ce/Al_2O_3. When this desorbed amount is expressed as % of the initially chemisorbed NH_3-s (before the NO/O_2/He gas switch), it is found that practically both catalysts desorb similar percentage, namely,

34–37% at 150 °C and 30–32% at 200 °C. This is an important result since it demonstrates that a significant surface coverage of adsorbed NH_3-s does not react with NO/O_2 in the 150–200 °C range. As indicated by the Py-FTIR (Fig. 8a) and *in situ* DRIFTS (Fig. 11) studies, $Ce_2/Cu_4Al_1O_x$ has a larger concentration of surface acid sites per gram basis than the other catalysts investigated, and Cu-Ce/Al_2O_3 shows significant concentration of strongly bound ammonia species (Fig. 8b). Thus, these results could explain well the larger amounts of NH_3 species desorbed during the NO/O_2 titration experiment (Fig. 15).

The initial very sharp transient response in the rate of N_2 formation observed at 200 °C for the $Ce_2/Cu_4Al_1O_x$ catalyst (Fig. 14B) might be used to argue that an E-R mechanism is likely to operate between adsorbed NH_3-s and NO (g). Further mechanistic studies about the NH_3-SCR of NO_x over the present catalytic systems are in progress using advanced SSITKA experiments to be reported in the near future. The latter experiments will probe the N-path from NO to the reaction products (N_2 and N_2O) by using labelled ^{15}NO (g), where the surface coverage of active NO_x, the mean residence time and their site reactivity under steady-state reaction conditions can be estimated [67,68]. Based on these results, some clues about E-R vs L-H mechanisms can be obtained.

3.6.3. Transient NO chemisorption (presence/absence of gaseous oxygen)

Fig. 16A and B show comparative specific transient rates (μmol $m^{-2}s^{-1}$) of NO consumption at 150 °C over Cu-Ce/Al_2O_3 (curve a) and $Ce_2/Cu_4Al_1O_x$-LDO (curve b) catalysts under the 1000 ppm NO/5%O_2/He and 1000 ppm NO/He gas mixture, respectively. During these NO gas treatments, small amounts of N_2O were formed but not any NO_2 (measured by mass spectrometry). Based on material balance (similar to Eq. (4)), the amounts (μmol g^{-1}) of NO_x-ads formed after the 20-min treatment in the NO/He or NO/O_2/He feed gas stream can be

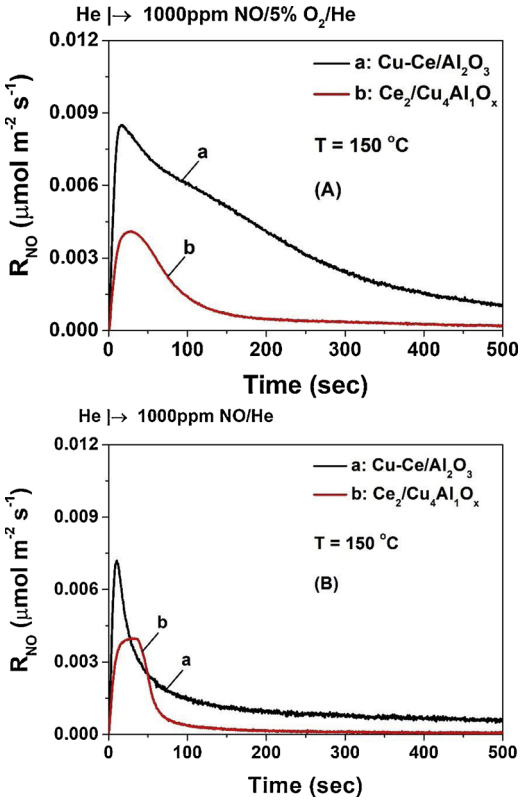

Fig. 16. Transient rates (μmol $m^{-2}s^{-1}$) of NO consumption as a function of time estimated after the step-gas switch (iii) He → 1000 ppm NO/5% O_2/1% Kr/Ar/He (t) (A) and step-gas switch (iv) He → 1000 ppm NO/1% Kr/Ar/He (t) (B) at T = 150 °C over a: Cu-Ce/Al_2O_3 and b: $Ce_2/Cu_4Al_1O_x$ catalysts; F_T = 50 N mL min^{-1}; W_{cat} = 0.05 g.

Table 3
Amounts (μmol g^{-1}) of NO consumed and N_2O produced for the $Ce_2/Cu_4Al_1O_x$-LDO and Cu-Ce/Al_2O_3 catalysts at T = 150 °C following the step-gas switch (iii) He → 1000 ppm NO/5% O_2/1% Kr/Ar/He (20 min) and the step-gas switch (iv) He → 1000 ppm NO/1% Kr/Ar/He (20 min).

Catalyst	Gas Switch	NO_{cons} (μmol g^{-1})	N_2O (μmol g^{-1})	NO_x-ads (μmol g^{-1})
Cu-Ce/Al_2O_3	(iv)	44.5	7.2	30.1
$Ce_2/Cu_4Al_1O_x$	(iv)	44.8	1.5	41.8
Cu-Ce/Al_2O_3	(iii)	137.7	3.5	130.7
$Ce_2/Cu_4Al_1O_x$	(iii)	93.7	12.8	68.1

estimated, and these are reported in Table 3 for the two catalytic systems. It should be noted that within less than 20 min on stream the NO gas signal in the mass spectrometer reached its feed value of 1000 ppm for both catalytic systems (NO_x-ads saturation). It is seen that significantly larger amounts of NO_x-ads are obtained when oxygen is co-fed with NO (see Table 3), and that NO_x adsorption on Cu-Ce/Al_2O_3 is larger by a factor of 1.92 compared to $Ce_2/Cu_4Al_1O_x$-LDO catalyst. Fig. 16A also illustrates that the shape of the transient rate of NO_x-ads formation is apparently different between the two catalytic surfaces. More precisely, a large shoulder at the initial period of chemisorption following the sharp maximum in the rate is observed on Cu-Ce/Al_2O_3, not seen in the case of $Ce_2/Cu_4Al_1O_x$-LDO catalyst. The latter may imply the formation of more kinds of NO_x-ads in the case of Cu-Ce/Al_2O_3. This result seems to be in harmony with the *in situ* DRIFTS reported in Fig. 10b,d for the same catalytic surfaces but after treatment with 2000 ppm NO/5%O_2/Ar gas mixture at 200 °C, where the IR band centered at 1608 cm^{-1} is accompanied by a shoulder on its low-frequency side in the case of Cu-Ce/Al_2O_3 (Fig. 10b), not seen in the case of $Ce_2/Cu_4Al_1O_x$-LDO (Fig. 10d). Of interest is the fact that in the absence of oxygen in the feed gas stream of NO, $Ce_2/Cu_4Al_1O_x$-LDO is able to provide larger amount of NO_x-ads species by a factor of ~ 1.4 compared to Cu-Ce/Al_2O_3 (Fig. 16B, Table 3), as opposed to the case of NO/O_2/He. Also, the two catalysts show completely different kinetics of NO_x formation (see shapes of R_{NO}, Fig. 16B).

Another important aspect of the NO/O_2 vs NO/He activity behavior of the two catalytic surfaces, is the amount of N_2O formed. In the case of NO/He gas treatment, the ratio of N_2O/NO_x-ads is 7% for $Ce_2/Cu_4Al_1O_x$ but 24% for Cu-Ce/Al_2O_3. On the other hand, in the case of NO/O_2/He gas treatment, this ratio is found to be 18.8 and 2.7%, respectively. This result is important since under NH_3-SCR at 150 °C, $Ce_2/Cu_4Al_1O_x$ has a slightly lower N_2O-selectivity than the Cu-Ce/Al_2O_3 catalyst. These results may imply that N_2O-selectivity is rather governed by surface reactions between adsorbed NH_x-s and NO_x-s species and not by the surface elementary reaction steps of NO/O_2 interaction.

3.6.4. Transient kinetics of NO_x-ads reaction in O_2 gas atmosphere

The reactivity of adsorbed NO_x-s species formed upon 1000 ppm NO/He gas treatment for 20 min at 150 °C (step-gas switch (iv), Fig. 16) towards 5%O_2/He gas was also investigated via the step-gas switch (v) (see Section 2.4), and results are presented in Fig. 17A–C. There is a clear decomposition of NO_x-s into gaseous NO (Fig. 17A) and reaction towards N_2O (Fig. 17B) and NO_2 (Fig. 17C) formation. The formation of N_2O and NO_2 was the result of reaction of NO_x-s with gaseous oxygen since the gas switch from NO/O_2/He to He instead to 5%O_2/He provided only NO and no N_2O and/or NO_2. This result is presented in Fig. S6 (ESI) in the case of Cu-Ce/Al_2O_3 catalyst, where after 7 min in He gas stream the amount of NO_x-ads decomposed to NO was 21 μmol g^{-1}.

Table 4 reports the quantities (μmol g^{-1}) of NO, N_2O and NO_2 obtained after 7 min of 5%O_2/He gas treatment of the catalysts (Fig. 17). Two important results need to be noted. The first one is the comparison of the transient response of N_2O formation under the 5%O_2/He gas treatment (7 min) with the amount of preadsorbed NO_x-s (see Table 3). The $Ce_2/Cu_4Al_1O_x$-LDO catalyst shows that only ~ 9.1% of adsorbed

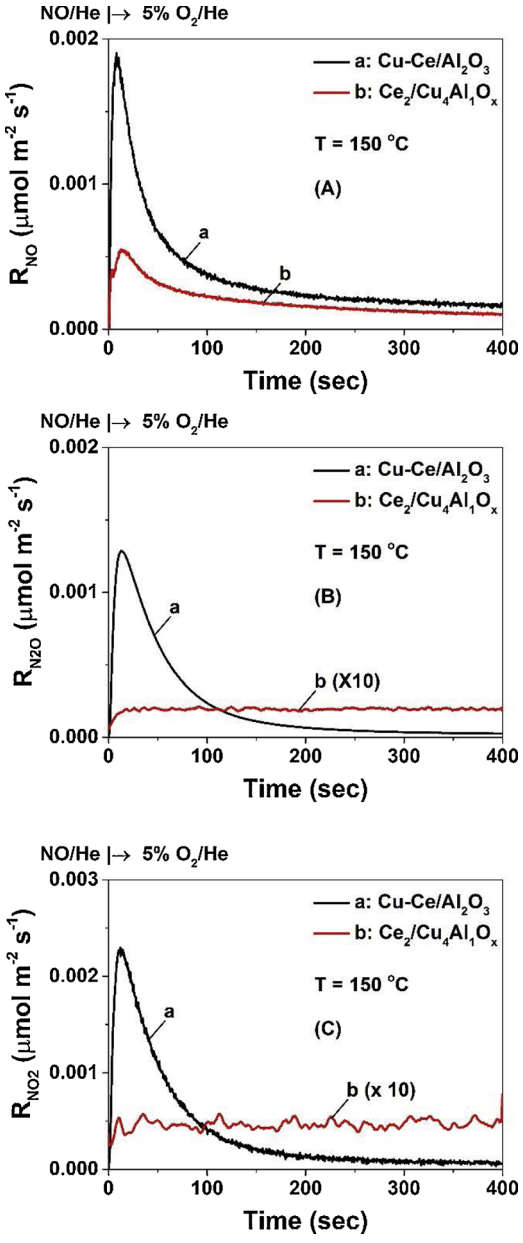

Fig. 17. Transient rates (μmol m^{-2} s^{-1}) of NO (A), N_2O (B) and NO_2 (C) formation as a function of time estimated under O_2/He at the step-gas switch (v) 1000 ppm NO/1% Kr/Ar/He (20 min) → 5% O_2/He (t) at T = 150 °C over a: Cu-Ce/Al_2O_3 and b: $Ce_2/Cu_4Al_1O_x$ catalysts; F_T = 50 N mL min^{-1}; W_{cat} = 0.05 g.

Table 4
Amounts (μmol g^{-1}) of NO, N_2O and NO_2 for the $Ce_2/Cu_4Al_1O_x$-LDO and Cu-Ce/Al_2O_3 catalysts at T = 150 °C following the step-gas switch (v) 1000 ppm NO/1% Kr/Ar/He (20 min) → 5% O_2/He (7 min).

Catalyst	NO (μmol g^{-1})	N_2O (μmol g^{-1})	NO_2 (μmol g^{-1})	Total NO_x -ads (μmol g^{-1})
Cu-Ce/Al_2O_3	9.9	5.4	7.1	27.8
$Ce_2/Cu_4Al_1O_x$	13.5	1.9	4.7	22.0

NO_x reacted to give N_2O, whereas in the case of Cu-Ce/Al_2O_3 this value is ~ 36%. This large difference in N_2O-selectivty is not in line with the NH_3-SCR results, and likely implies that N_2O-selctivity in NH_3-SCR is rather determined exclusively by the different kinetics operated under the catalyst surface composition of adsorbed *active* species that are found in the N-pathway of forming N_2O. Alternatively, the N_2O formation rate of NO_x-s with gaseous oxygen is suppressed under NH_3-SCR for the Cu-Ce/Al_2O_3 catalyst. As shown in Fig. 17B, the transient response of N_2O formation is completely different in shape for the two catalysts. A very similar shape of the N_2O response obtained on the $Ce_2/Cu_4Al_1O_x$-LDO (practically constant rate after 7 min on O_2/He gas stream) was reported by Zhang et al. [43] on a fully oxidized CeO_2 after the switch N_2 → 500 ppm NH_3/N_2 gas mixture at 350 °C.

The second important result relates to the rate and kinetics of NO_2 formation. As shown in Fig. 17C, totally different shape in the response of NO_2 formation rate is obtained for the two catalyst compositions, as in the case of N_2O response discussed in the previous paragraph. In the case of Cu-Ce/Al_2O_3, a sharp peak maximum in the rate is obtained upon the O_2/He gas switch, which decays quickly (within the first 200 s) to a very low value. On the other hand, the transient rate of NO_2 on the $Ce_2/Cu_4Al_1O_x$-LDO catalyst takes immediately a low value (~ 42 times lower than the initial rate of Cu-Ce/Al_2O_3 catalyst), which practically decays very slowly for the first 7 min on the O_2/He gas stream; it is noted that on a gram basis, this difference in the initial rates of NO_2 formation drops to a factor of ~ 16, as the result of the SSA (m^2 g^{-1}) differences in the two catalyst samples. However, the amount of NO_2 formed (μmol g^{-1}; 7 min of reaction) is only ~ 1.5 times lower than that formed by the Cu-Ce/Al_2O_3 catalyst. Furthermore, the percentage of adsorbed NO_x-s leading to NO_2 upon exposure to the O_2/He (7 min) is 21.3 and 25.5% for the $Ce_2/Cu_4Al_1O_x$-LDO and Cu-Ce/Al_2O_3 catalysts, respectively. These results indicate that the reactivity of NO_x-s towards O_2 to form NO_2 is significantly larger on Cu-Ce/Al_2O_3 compared to the $Ce_2/Cu_4Al_1O_x$-LDO catalyst. On the other hand, it is very important to mention at this point that under real NH_3-SCR conditions it is to be speculated whether this difference in reactivity would be still observed. Also, it is important to understand whether $Ce_2/Cu_4Al_1O_x$-LDO is more efficient to adsorb NO_2 than Cu-Ce/Al_2O_3, and therefore this might be the reason of measuring lower rates of gaseous NO_2 formation during the O_2/He gas treatment. These issues requires further future investigations regarding transient chemisorption of NO_2 with mass spectrometer and *in situ* DRIFTS, subject out of the scope of the present work.

4. Conclusions

We reported a novel $Ce_2/Cu_4Al_1O_x$-layered double oxide (LDO) catalyst containing copper and cerium species as active components obtained after calcination at 400 °C of Ce_2/Cu_4Al_1O-CO_3 LDH precursors. The $Ce_2/Cu_4Al_1O_x$-LDO showed 95.3% NH_3-SCR NO_x conversion at 200 °C, which was higher than the maximum de-NO_x efficiency of Cu/Al_2O_3 (82.6%) and Cu-Ce/Al_2O_3 (87.9%) prepared by the wet-impregnation technique. Significantly larger activity differences were obtained at lower temperatures (ca. 150 °C). However, the $Ce_2/Cu_4Al_1O_x$-LDO showed at the same time much better resistance to the co-presence of SO_2, HCl and H_2O in the NH_3-SCR reaction feed gas stream, indicating the potential of this material for practical applications.

Powder XRD and XPS analyses indicated that $Ce_2/Cu_4Al_1O_x$ catalyst possessed highly dispersed Cu^{2+} and Ce^{3+} species, which it is believed to play a key role in the promotion of the rate of NH_3-SCR. In addition, Py-FTIR, NH_3-TPD and H_2-TPR results showed that $Ce_2/Cu_4Al_1O_x$ has a larger concentration of surface acid sites and higher reduction potential compared with the other Cu-Ce-Al-O_x - based catalysts investigated. According to H_2-TPR, ICS and in-situ DRIFTS analyses, after HCl/SO_2 gas poisoning treatment, the redox properties of $Ce_2/Cu_4Al_1O_x$ were significantly less affected, and lower amounts of metal sulfate and metal chloride species were formed, thus proving its exhibited poisoning resistance.

Transient ammonia chemisorption followed by NO/O_2 reaction of pre-adsorbed ammonia revealed important information about some intrinsic kinetic reasons for the observed enhanced activity of $Ce_2/Cu_4Al_1O_x$ compared to that of Cu-Ce/Al_2O_3 catalyst. In particular, the

site reactivity (k, s^{-1}) and not the surface coverage of active NH_x-s intermediates dictates the rate of NH_3-SCR. In addition, $Ce_2/Cu_4Al_1O_x$ presented activated sites for ammonia chemisorption which may not be of importance in the NH_3-SCR as opposed to the Cu-Ce/Al_2O_3 catalyst.

Transient NO chemisorption at 150 °C in the absence and presence of gaseous oxygen (5 vol%) followed by reactivity studies of the formed NO_x-s with 5%O_2/He revealed that the N_2O-selectivtiy in NH_3-SCR is largely determined by the surface catalytic chemistry of adsorbed NH_x-s and NO_x-s (or gaseous NO) and not by surface reactions of NO_x-s with gaseous O_2.

Acknowledgements

This work was supported by the National Natural Science Foundation of China (U1810209, 51572029, 51622801) and the Beijing Natural Science Foundation (2184114). The Research Committee of the University of Cyprus is also acknowledged for financial support.

Appendix A. Supplementary data

Supplementary material related to this article can be found, in the online version, at doi:https://doi.org/10.1016/j.apcatb.2019.117749.

References

[1] H.-H. Tseng, C.-Y. Lu, F.-Y. Chang, M.-Y. Wey, H.-T. Cheng, Catalytic removal of NO and PAHs over AC-supported catalysts from incineration flue gas: bench-scale and pilot-plant tests, Chem. Eng. J. 169 (2011) 135–143.
[2] L. Luo, Y. Guo, T. Zhu, Y. Zheng, Adsorption species distribution and multi-component adsorption mechanism of SO_2, NO and CO_2 on commercial adsorbents, Energy Fuel 31 (2017) 11026–11033.
[3] Q. Yan, S. Chen, L. Qiu, Y. Gao, D. O'Hare, Q. Wang, The synthesis of $Cu_yMn_zAl_{1-z}O_x$ mixed oxide as a low-temperature NH_3-SCR catalyst with enhanced catalytic performance, Dalton Trans. 47 (2018) 2992–3004.
[4] C. Shi, H. Chang, C. Wang, T. Zhang, Y. Peng, M. Li, Y. Wang, J. Li, Improved activity and H_2O resistance of Cu-modified MnO_2 catalysts for NO oxidation, Ind. Eng. Chem. Res. 57 (2018) 920–926.
[5] F.-Y. Chang, M.-Y. Wey, J.-C. Chen, Effects of sodium modification, different reductants and SO_2 on NO reduction by Rh/Al_2O_3 catalysts at excess O_2 conditions, J. Hazard. Mater. 156 (2008) 348–355.
[6] F.-Y. Chang, J.-C. Chen, M.-Y. Wey, Activity and characterization of Rh/Al_2O_3 and Rh–Na/Al_2O_3 catalysts for the SCR of NO with CO in the presence of SO_2 and HCl, Fuel 89 (2010) 1919–1927.
[7] R. Zhang, N. Liu, Z. Lei, B. Chen, Selective transformation of various nitrogen-containing exhaust gases toward N_2 over zeolite catalysts, Chem. Rev. 116 (2016) 3658–3721.
[8] N. Fang, J. Guo, S. Shu, H. Luo, Y. Chu, J. Li, Enhancement of low-temperature activity and sulfur resistance of $Fe_{0.3}Mn_{0.5}Zr_{0.2}$ catalyst for NO removal by NH_3-SCR, Chem. Eng. J. 325 (2017) 114–123.
[9] H. Chang, T. Zhang, H. Dang, X. Chen, Y. You, J.W. Schwank, J. Li, Fe_2O_3@SiTi core-shell catalyst for the selective catalytic reduction of NO_x with NH_3: activity improvement and HCl tolerance, Catal. Sci. Technol. 8 (2018) 3313–3320.
[10] F. Gao, X. Tang, H. Yi, J. Li, S. Zhao, J. Wang, C. Chu, C. Li, Promotional mechanisms of activity and SO_2 tolerance of Co- or Ni-doped MnO_x-CeO_2 catalysts for SCR of NO_x with NH_3 at low temperature, Chem. Eng. J. 317 (2017) 20–31.
[11] J.-C. Chen, M.-Y. Wey, C.-L. Yeh, Y.-S. Liang, Simultaneous treatment of organic compounds, CO, and NO_x in the incineration flue gas by three-way catalyst, Appl. Catal. B: Environ. 48 (2004) 25–35.
[12] T. Zhang, H. Chang, K. Li, Y. Peng, X. Li, J. Li, Different exposed facets VO_x/CeO_2 catalysts for the selective catalytic reduction of NO with NH_3, Chem. Eng. J. 349 (2018) 184–191.
[13] X. Du, X. Gao, L. Cui, Y. Fu, Z. Luo, K. Cen, Investigation of the effect of Cu addition on the SO_2-resistance of a Ce-Ti oxide catalyst for selective catalytic reduction of NO with NH_3, Fuel 92 (2012) 49–55.
[14] Z. Chen, Q. Yang, H. Li, X. Li, L. Wang, S.C. Tsang, Cr-MnO_x mixed-oxide catalysts for selective catalytic reduction of NO_x with NH_3 at low temperature, J. Catal. 276 (2010) 56–65.
[15] W. Yao, Y. Liu, Z. Wu, The promoting effect of CeO_2@Ce-O-P multi-core@shell structure on SO_2 tolerance for selective catalytic reduction of NO with NH_3 at low temperature, Appl. Surf. Sci. 442 (2018) 156–163.
[16] Z. Lian, F. Liu, W. Shan, H. He, Improvement of Nb doping on SO_2 resistance of VO_x/CeO_2 catalyst for the selective catalytic reduction of NO_x with NH_3, J. Phys. Chem. C 121 (2017) 7803–7809.
[17] I. Salem, X. Courtois, E.C. Corbos, P. Marecot, D. Duprez, NO conversion in presence of O_2, H_2O and SO_2: improvement of a Pt/Al_2O_3 catalyst by Zr and Sn, and influence of the reducer C_3H_6 or C_3H_8, Catal. Commun. 9 (2008) 664–669.
[18] J.W. Choung, I.S. Nam, Characteristics of copper ion exchanged mordenite catalyst deactivated by HCl for the reduction of NO_x with NH_3, Appl. Catal. B: Environ. 64 (2006) 42–50.
[19] J.W. Choung, I.S. Nam, Role of cerium in promoting the stability of CuHM catalyst against HCl to reduce NO with NH_3, Appl. Catal. A: Gen. 312 (2006) 165–174.
[20] G.G. Park, H.J. Chae, I.S. Nam, J.W. Choung, K.H. Choi, Deactivation of mordenitetype zeolite catalyst by HCl for the reduction of NO_x with NH_3, Microporous Mesoporous Mater. 48 (2001) 337–343.
[21] H. Chang, Q. Wu, T. Zhang, M. Li, X. Sun, J. Li, L. Duan, J. Hao, Design strategies for CeO_2-MoO_3 catalysts for DeNO$_x$ and Hg^0 oxidation in the presence of HCl: the significance of the surface acid–base properties, Environ. Sci. Technol. 49 (2015) 12388–12394.
[22] X. She, M. Flytzani-Stephanopoulos, Activity and stability of Ag-alumina for the selective catalytic reduction of NO_x with methane in high-content SO_2 gas streams, Catal. Today 127 (2007) 207–218.
[23] G. Xie, Z. Liu, Z. Zhu, Q. Liu, J. Ge, Z. Huang, Simultaneous removal of SO_2 and NO_x from flue gas using a CuO/Al_2O_3 catalyst sorbent: I. Deactivation of SCR activity by SO_2 at low temperatures, J. Catal. 224 (2004) 36–41.
[24] H. Zhang, M.U. Tahir, X. Yan, X. Liu, X. Su, L. Zhang, Ni-Al layered double hydroxide with regulated interlayer spacing as electrode for aqueous asymmetric supercapacitor, Chem. Eng. J. 368 (2019).
[25] H.A. Lara-García, W. Gao, A. Gómez-Cortés, G. Díaz, H. Pfeiffer, Q. Wang, High and efficient CO_2 capture in molten nitrates modified Mg-Al-palmitate layered double oxides at high pressures and elucidation of carbonation mechanisms by in situ DRIFT spectroscopy analysis, Ind. Eng. Chem. Res. 58 (2019) 5501–5509.
[26] T. Xue, R. Li, W. Gao, Y. Gao, Q. Wang, A. Umar, Preparation and characterization of highly efficient CuFe mixed oxides for total oxidation of toluene, J. Nanosci. Nanotechnol. 18 (2018) 3381–3386.
[27] P. Lu, Y. Liu, T. Zhou, Q. Wang, Y. Li, Recent advances in layered double hydroxides (LDHs) as two-dimensional membrane materials for gas and liquid separations, J. Membrane Sci. 567 (2018) 89–103.
[28] Q. Yan, S. Chen, C. Zhang, Q. Wang, B. Louis, Synthesis and catalytic performance of $Cu_1Mn_{0.5}Ti_{0.5}O_x$ mixed oxide as low-temperature NH_3-SCR catalyst with enhanced SO_2 resistance, Appl. Catal. B: Environ. 238 (2018) 236–247.
[29] J. Wang, X. Mei, L. Huang, Q. Zheng, Y. Qiao, K. Zang, S. Mao, R. Yang, Z. Zhang, Y. Gao, Z. Guo, Z. Huang, Q. Wang, Synthesis of layered double hydroxides/graphene oxide nanocomposite as novel high-temperature CO_2 adsorbent, J. Energy Chem. 24 (2015) 127–137.
[30] Q. Qin, J. Wang, T. Zhou, Q. Zheng, L. Huang, Y. Zhang, P. Lu, A. Umar, B. Louis, Q. Wang, Impact of organic interlayer anions on the CO_2 adsorption performance of Mg-Al layered double hydroxides derived mixed oxides, J. Energy Chem. 26 (2017) 346–353.
[31] T. Baidya, A. Gupta, P.A. Deshpandey, G. Madras, M.S. Hegde, High oxygen storage capacity and high rates of CO oxidation and NO reduction catalytic properties of $Ce_{1-x}Sn_xO_2$ and $Ce_{0.78}Sn_{0.2}Pd_{0.02}O_{2-\delta}$, J. Phys. Chem. C 113 (2009) 4059–4068.
[32] M. Adamowska, A. Krztoń, M. Najbar, P. Da Costa, G. Djéga-Mariadassou, DRIFT study of the interaction of NO and O_2 with the surface of $Ce_{0.62}Zr_{0.38}O_2$ as deNO$_x$ catalyst, Catal. Today 137 (2008) 288–291.
[33] C.A. Emeis, Determination of integrated molar extinction coefficients for infrared absorption bands of pyridine adsorbed on solid acid catalysts, J. Catal. 141 (1993) 347–354.
[34] C.N. Costa, S.Y. Christou, G. Georgiou, A.M. Efstathiou, Mathematical modeling of the oxygen storage capacity phenomenon studied by CO pulse transient experiments over Pd/CeO_2 catalyst, J. Catal. 219 (2003) 259–272.
[35] Q. Wang, H.H. Tay, D.J.W. Ng, L. Chen, Y. Liu, J. Chang, Z. Zhong, J. Luo, A. Borgna, The effect of trivalent cations on the performance of Mg-M-CO3 layered double hydroxides for high-temperature CO_2 capture, ChemSusChem 3 (2010) 965–973.
[36] Q. Wang, X. Zhang, C.J. Wang, J. Zhu, Z. Guo, D. O'Hare, Polypropylene/layered double hydroxide nanocomposites, J. Mater. Chem. 22 (2012) 19113–19121.
[37] C. Gennequin, T. Barakat, H.L. Tidahy, R. Cousin, J.F. Lamonier, A. Aboukaïs, S. Siffert, Use and observation of the hydrotalcite "memory effect" for VOC oxidation, Catal. Today 157 (2010) 191–197.
[38] L. Xu, C. Wang, H. Chang, Q. Wu, T. Zhang, J. Li, New Insight into SO_2 poisoning and regeneration of CeO_2-WO_3/TiO_2 and V_2O_5-WO_3/TiO_2 catalysts for low-temperature NH_3-SCR, Environ. Sci. Technol. 52 (2018) 7064–7071.
[39] B. Jiang, Y. Liu, Z. Wu, Low-temperature selective catalytic reduction of NO on MnO_x/TiO_2 prepared by different methods, J. Hazard. Mater. 162 (2009) 1249–1254.
[40] M. Yu, C. Li, G. Zeng, Y. Zhou, X. Zhang, The selective catalytic reduction of NO with NH_3 over a novel Ce-Sn-Ti mixed oxides catalyst: promotional effect of SnO_2, Appl. Surf. Sci. 342 (2015) 174–182.
[41] F.-Y. Chang, J.-C. Chen, M.-Y. Wey, Catalytic removal of NO in waste incineration processes over Rh/Al_2O_3 and Rh-Na/Al_2O_3: effects of particulates, heavy metals, SO_2 and HCl, Fuel Process. Technol. 90 (2009) 576–582.
[42] W. Shan, F. Liu, H. He, X. Shi, C. Zhang, Novel cerium-tungsten mixed oxide catalyst for the selective catalytic reduction of NO_x with NH_3, Chem. Commun. 47 (2011) 8046–8048.
[43] L. Zhang, J. Pierce, V.L. Leung, D. Wang, W.S. Epling, Characterization of Ceria's interaction with NO_x and NH_3, J. Phys. Chem. C 117 (2013) 8282–8289.
[44] Q. Yan, Y. Nie, R. Yang, Y. Cui, D. O'Hare, Q. Wang, Highly dispersed $CuyAlO_x$ mixed oxides as superior low-temperature alkali metal and SO_2 resistant NH_3-SCR catalysts, Appl. Catal. A: Gen. 538 (2017) 37–50.
[45] P. Burroughs, A. Hamnett, A.F. Orchard, G. Thornton, Satellite structure in the X-ray photoelectron spectra of some binary and mixed oxides of lanthanum and cerium, J. Chem. Soc. Dalton Trans. 17 (1976) 1686–1698.
[46] L.J. Yan, Y.Y. Liu, K.W. Zha, H.R. Li, L.Y. Shi, D.S. Zhang, Deep insight into the structure-activity relationship of Nb modified SnO_2-CeO_2 catalysts for low-

temperature selective catalytic reduction of NO by NH_3, Catal. Sci. Technol. 7 (2017) 502–514.
[47] C. Fang, D. Zhang, S. Cai, L. Zhang, L. Huang, H. Li, P. Maitarad, L. Shi, R. Gao, J. Zhang, Low-temperature selective catalytic reduction of NO with NH_3 over nanoflaky MnO_x on carbon nanotubes in situ prepared via a chemical bath deposition route, Nanoscale 5 (2013) 9199–9207.
[48] L. Chen, J. Li, M. Ge, The poisoning effect of alkali metals doping over nano V_2O_5-WO_3/TiO_2 catalysts on selective catalytic reduction of NO_x by NH_3, Chem. Eng. J. 170 (2011) 531–537.
[49] F. Liu, H. He, C. Zhang, Z. Feng, L. Zheng, Y. Xie, T. Hu, Selective catalytic reduction of NO with NH_3 over iron titanate catalyst: catalytic performance and characterization, Appl. Catal. B: Environ. 96 (2010) 408–420.
[50] S. Ali, L. Chen, F. Yuan, R. Li, T. Zhang, S.H. Bakhtiar, X. Leng, X. Niu, Y. Zhu, Synergistic effect between copper and cerium on the performance of Cu_x-$Ce_{0.5-x}$-$Zr_{0.5}$ (x = 0.1–0.5) oxides catalysts for selective catalytic reduction of NO with ammonia, Appl. Catal. B: Environ. 210 (2017) 223–234.
[51] M.I. Zaki, M.A. Hasan, F.A. Al-Sagheer, L. Pasupulety, In situ FTIR spectra of pyridine adsorbed on SiO_2-Al_2O_3, TiO_2, ZrO_2 and CeO_2: general considerations for the identification of acid sites on surfaces of finely divided metal oxides, Colloid. Surf. A 190 (2001) 261–274.
[52] D.A. Peña, B.S. Uphade, P.G. Smirniotis, TiO_2-supported metal oxide catalysts for low-temperature selective catalytic reduction of NO with NH_3: I. Evaluation and characterization of first row transition metals, J. Catal. 221 (2004) 421–431.
[53] Y. Yang, M. Wang, Z. Tao, Q. Liu, Z. Fei, X. Chen, Z. Zhang, J. Tang, M. Cui, X. Qiao, Mesoporous Mn-Ti amorphous oxides: a robust low-temperature NH_3-SCR catalyst, Catal. Sci. Technol. 8 (2018) 6396–6406.
[54] Y. Zhang, X. Zhao, H. Xu, K. Shen, C. Zhou, B. Jin, K. Sun, Novel ultrasonic-modified MnO_x/TiO_2 for low-temperature selective catalytic reduction (SCR) of NO with ammonia, J. Colloid Interface Sci. 361 (2011) 212–218.
[55] P.G. Smirniotis, D.A. Peña, B.S. Uphade, Low-temperature selective catalytic reduction (SCR) of NO with NH_3 by using Mn, Cr, and Cu oxides supported on hombikat TiO_2, Angew. Chem. Int. Ed. 40 (2001) 2479–2481.
[56] N. Yang, R. Guo, W. Pan, Q. Chen, Q. Wang, C. Lu, S. Wang, The deactivation mechanism of Cl on Ce/TiO_2 catalyst for selective catalytic reduction of NO with NH_3, Appl. Surf. Sci. 378 (2016) 513–518.
[57] R. Jin, Y. Liu, Z. Wu, H. Wang, T. Gu, Relationship between SO_2 poisoning effects and reaction temperature for selective catalytic reduction of NO over Mn-Ce/TiO_2 catalyst, Catal. Today 153 (2010) 84–89.
[58] L. Chen, J. Li, M. Ge, DRIFT study on cerium-tungsten/titiania catalyst for selective catalytic reduction of NO_x with NH_3, Environ. Sci. Technol. 44 (2010) 9590–9596.
[59] J. Eng, C.H. Bartholomew, Kinetic and mechanistic study of NO_x reduction by NH_3 over H-form zeolites, J. Catal. 171 (1997) 27–44.
[60] L. Zhang, D. Wang, Y. Liu, K. Kamasamudram, J. Li, W.S. Epling, SO_2 poisoning impact on the NH_3-SCR reaction over a commercial Cu-SAPO-34 SCR catalyst, Appl. Catal. B: Environ. 156–157 (2014) 371–377.
[61] X. Jiang, P. Lu, C. Li, Z. Zeng, G. Zeng, L. Hu, L. Mai, Z. Li, Experimental study on a room temperature urea-SCR of NO over activated carbon fibre-supported CeO_2-CuO, Environ. Technol. 34 (2013) 591–598.
[62] L. Zhang, L. Li, Y. Cao, X. Yao, C. Ge, F. Gao, Y. Deng, C. Tang, L. Dong, Getting insight into the influence of SO_2 on TiO_2/CeO_2 for the selective catalytic reduction of NO by NH_3, Appl. Catal. B: Environ. 165 (2015) 589–598.
[63] Z. Fan, J. Shi, C. Gao, G. Gao, B. Wang, Y. Wang, C. He, C. Niu, Gd-modified MnO_x for the selective catalytic reduction of NO by NH_3: the promoting effect of Gd on the catalytic performance and sulfur resistance, Chem. Eng. J. 348 (2018) 820–830.
[64] S.D. Lin, A.C. Gluhoi, B.E. Nieuwenhuys, Ammonia oxidation over $Au/MO_x/\gamma$-Al_2O_3-activity, selectivity and FTIR measurements, Catal. Today 90 (2004) 3–14.
[65] Q. Zhang, J. Fan, P. Ning, Z. Song, X. Liu, L. Wang, J. Wang, H. Wang, K. Long, In situ DRIFTS investigation of NH_3-SCR reaction over CeO_2/zirconium phosphate catalyst, Appl. Surf. Sci. 435 (2018) 1037–1045.
[66] Y. Chen, J. Wang, Z. Yan, L. Liu, Z. Zhang, X. Wang, Promoting effect of Nd on the reduction of NO with NH_3 over CeO_2 supported by activated semi-coke: an in situ DRIFTS study, Catal. Sci. Technol. 5 (2015) 2251–2259.
[67] A.M. Efstathiou, J.T. Gleaves, G.S. Yablonsky, Transient techniques: temporary analysis of products (TAP) and steady state isotopic transient kinetic analysis (SSITKA), in: M. Che, J.C. Vedrine (Eds.), Characterization of Solid Materials and Heterogeneous Catalysts From Structure to Surface Reactivity, Wiley-VCH, 2012, pp. 1013–1073.
[68] A.M. Efstathiou, K. Fliatoura, The selective catalytic reduction of NO with NH_3 over V_2O_5/TiO_2 catalyst: a steady-state and transient kinetic study, Appl. Catal. B: Environ. 6 (1995) 35–59.